Tim Palmer elected a Fellow of the Royal Society

We are delighted to hear that Tim Palmer (Head of the Probability Forecasting and Diagnostics Division) was elected as a Fellow of the Royal Society on 15 May 2003.

Tim is distinguished for his world-leading contributions in a number of high-profile areas in atmospheric science. His research benefits from the ability to cross-fertilise between disciplines, and from his insight and his gift for communication. He took the key initiative towards a breakthrough to modern thinking about the dynamics of the stratosphere and the ozone layer in terms of planetary-wave propagation and breaking. His work on representing in weather-prediction and climate models the drag due to breaking gravity waves has been highly influential. Tim has also established himself as a world leader in exploiting non-linear dynamical-system concepts and sophisticated mathematical methods, in combination with numerical experiments using large atmospheric models, for predicting the predictability of weather and for probing the reasons for, and the possible prediction of, interannual and interdecadal climatic variability.

The Royal Society is the world's oldest scientific academy in continuous existence. It was founded in 1660, and received its Royal Charter from King Charles II. It is an independent body and its 1300 Fellows and Foreign Members are eminent scientists (including some 65 Nobel Laureates) representing the full range of scientific disciplines. A maximum of 42 Fellows may be elected annually.

The Royal Society has the lead role in promoting the interests of science and technology in interactions with the UK government, the public and the media. Fellows are elected for their distinguished contributions to science, engineering or technology, either through fundamental research or through leading and directing scientific and technological progress in industry and research establishments. Election to Fellowship of the Royal Society is regarded as the highest scientific accolade that can be bestowed in the United Kingdom.

We would like to offer our congratulations to Tim on the achievement of this honour.

Adrian Tompkins wins the L.F. Richardson Prize

Adrian Tompkins has been awarded the Royal Meteorological Society's L.F. Richardson Prize for 2003. The L.F. Richardson Prize (instituted in memory of the pioneer of numerical weather prediction, Lewis Fry Richardson) is awarded for an outstanding paper published in the Society's journals by a young scientist (under the age of 30 at the time of the paper's submission).

Adrian was awarded the Prize (jointly with Ellie Highwood (University of Reading)) for his paper published in the Quarterly Journal on radiative-convective equilibrium in a three-dimensional cloud-ensemble model (published with co-author Dr. George Craig). A set of innovatively designed numerical simulations provided estimates of the rate of equilibration of tropical atmospheric structure resulting from deep convective activity. The modelled equilibrium state was shown to be consistent with appropriate tropical observations. This research provides a key insight into the processes responsible for such equilibration, as well as addressing the issue of convective self-organization. This well-cited paper is noteworthy in significantly improving our basic understanding of the tropical atmosphere. Congratulations to Adrian on this award.

In this issue

European Centre for Medium-Range Weather Forecasts

Shinfield Park, Reading, Berkshire RG2 9AX, UK

Fax: . . . . . .+44 118 986 9450

Telephone: National 0118 949 9000

International . . . . . .+44 118 949 9000

ECMWF Web site . . . . . .http://www.ecmwf.int

The ECMWF Newsletter is published quarterly and contains articles about new developments and systems at ECMWF. Articles about uses and applications of ECMWF forecasts are also welcome from authors working elsewhere (especially those from Member States and Co-operating States).

The ECMWF Newsletter is not a peer-reviewed publication.

Editor: Peter White

Typesetting and Graphics: Rob Hine

Front Cover

A tornado near Manchester, South Dakota on 24 June 2003. The article on page 8 discusses forecasts of severe convection associated with a tornado outbreak in the USA in summer 2003.

Photograph © Mike Berger/Jim Reed Photography (www.jimreedphoto.com).

Editorial

The article on page 2 gives details of a project spearheaded by Italian scientists (in cooperation with ECMWF) to use limited-area ensemble forecasts to improve the prediction of local precipitation; the success of the scheme is illustrated by an example of heavy rainfall that occurred in northern Italy in November 2002. The forecasting of severe convection, such as the events that led to the widespread outbreak of damaging tornadoes in the USA during May 2003, is discussed on page 8 by Peter Bechtold and colleagues. They highlight the usefulness of the Ensemble Prediction System for estimating the probability of such severe events occurring.

The new ECMWF seasonal forecasting system is described in the article on page 17 by David Anderson, Tim Stockdale, Laura Ferranti and Magdalena Balmaseda. There are plans to include the Met Office model in the system in the near future. Geert Jan van Oldenborgh and colleagues examine the comparative performances of the ECMWF seasonal forecasting system and of a simple statistical model on page 26, and on page 30 Federico Grazzini and Pedro Viterbo draw attention to the anomalously high sea surface temperatures in the Mediterranean (and around Scandinavia) at the time of writing (August 2003) and they point out that such anomalies can lead to heavy rainfall and intense cyclogenesis later in the year.

A short article on page 32 by Matteo Dell'Acqua provides details of new features of ECaccess (previously discussed in detail in ECMWF Newsletter 96 Winter 2002/03 page 28).

Peter White

Changes to the Operational Forecasting System

Cycle 26r1 was introduced on 29 April 2003. This was only a technical change and involved the writing of observations directly into the Observation Data Base (ODB).

Planned changes

A new version is under pre-operational testing (Cycle 26r3). It involves:

- A new formulation of the humidity analysis;
- New data streams (mostly AIRS, but also AMSU-B, AQUA AMSU-A, Japanese profilers, Meteosat5, GOES9 and GOES12 WV clear-sky radiances, GOES12 winds and MIPAS ozone-profile retrievals);
- A new linear radiation scheme in 4D-var, a new radiation sampling (HALO) and a new aerosol climatology;
- A relaxation of the convective mass-flux limiter for long time steps;
- New products (UVB, CAPE, photosynthetically active radiation).

François Lalaurette

Operational limited-area ensemble forecasts based on the 'Lokal Modell'

Increases in computer power in recent years have enabled a marked improvement in numerical weather-prediction (NWP) models allowing, not only the possibility of higher horizontal and vertical resolution, but also of a more detailed description of the physical processes related to atmospheric instability. As a consequence, the average performance of NWP models is becoming noticeably better and the operational use of sophisticated global-model ensemble prediction systems is becoming more widespread. Nevertheless, the forecasting of localised and severe-weather events (e.g. heavy rainfall, strong winds, cold-temperature anomalies) is still a challenging problem (mesoscale and orography-related processes can seriously limit the predictability of intense and localised events) despite more careful detection of the precursors and a better understanding of the development and mature phases of these kinds of phenomena. Although the use of high-resolution limited-area models (LAMs) nested in global-model runs has definitely improved the short-range prediction of locally intense events, it is sometimes difficult to forecast accurately their spatio-temporal evolution for ranges longer than 48 hours. Therefore, several methodologies have recently been experimented with and implemented to address the problem of improving short-to-medium-range prediction of those surface fields heavily affected by local processes (the attention being often focused on quantitative precipitation forecasts (QPF)). Thanks to the generation of ensemble prediction systems, many weather centres have given much more emphasis to the probabilistic approach, which enables the predictability of the atmospheric flow to be estimated for assessing the reliability of deterministic forecasts beyond the very short range.

Development of targeted ensemble prediction systems

In November 2000 ECMWF increased the horizontal resolution of the operational ensemble prediction system (EPS) from approximately 120 km to 80 km (i.e. from T159L40 to T255L40) in order to enhance the description of orography-related processes. A stochastic forcing in the physical parameterisation of the ECMWF model has also been introduced to account for model errors and to increase the EPS spread. In recent years, ECMWF has also developed a targeted ensemble prediction system (TEPS), where the perturbations differentiating the initial conditions of the ensemble system are given by linear combinations of singular vectors targeted to maximize the 48-hour total-energy perturbation over areas such as the European area, instead of only the extratropical Northern and Southern Hemispheres. A joint research group, including the Regional Meteorological Service of Emilia-Romagna ARPA-SMR, the Royal Netherlands Meteorological Institute and Oslo University, carried out a verification program to test the validity of running a TEPS system to provide initial and boundary conditions to limited-area models, as well as to improve the probabilistic predictability of heavy-rainfall events (that is, precipitation accumulations greater than 20 mm/day) with a global model. During 1999, TEPS experimentation started as a special project at ECMWF and targeted ensembles were run twice a week (on Fridays and Sundays). The probabilistic prediction of heavy-rainfall events over Europe was slightly better for TEPS than for the standard EPS over ranges between 72 and 96 hours. Tests of the validity of running TEPS to provide initial and boundary conditions for limited-area integrations have been encouraging. A 'poor man's EPS', obtained by using an ensemble of forecasts from different weather centres has also been proposed. Model uncertainties are implicitly considered in this approach, and it provides reliable probabilistic forecasts, both in the short and medium ranges.

A short-range ensemble forecasting system has been implemented at NCEP, USA; it is composed of 15 integrations of the ETA model and of the regional spectral model, and provides QPFs for ranges up to 63 hours. The Norwegian National Meteorological Institute has experimented with a limited-area ensemble generated by nesting their operational limited-area model in each member of a 21-member TEPS ensemble. This approach (sometimes referred to as the 'brute-force' approach) appears to provide better results than TEPS for the prediction of heavy-rainfall events, though at the cost of such an increased computational burden as to make it unaffordable on an operational basis, at least for the time being.

The limited-area ensemble prediction system - LEPS

Researchers at ARPA-SMR have developed a limited-area ensemble prediction system (LEPS). The ensemble members of the ECMWF EPS are first grouped into five clusters, and then a representative member (RM) is selected within each cluster (*Marsigli et al.* 2001; *Molteni et al.* 2001). The RMs provide both the initial and boundary conditions for integrations with a limited-area model, which is run five times (once per RM), so generating a small-size high-resolution ensemble for forecast ranges up to 120 hours. Hence, the probabilistic products typically generated at ECMWF (e.g. probability maps for rainfall rates or wind intensities exceeding particular thresholds) can be produced on the basis of the information provided by LAM integrations, each run being weighted according to the population of the cluster from which the RM is selected[1]. Another important feature of LEPS is the use of 'super-ensembles'. Rather than just using a set of forecasts from only one ECMWF EPS run, three consecutive EPS sets progressively lagged in time are used, providing initial ensembles of 153 individual members for the current operational implementation of EPS. From preliminary evaluations, the use of the super-ensemble technique

1 It is worth mentioning that the experimentation was carried out using LAMBO (Limited Area Model BOlogna), the hydrostatic limited-area model in operational use at ARPA-SMR. LAMBO is based on the NCEP ETA model and has an operational horizontal resolution of 20 km with 32 vertical levels.

increases the reliability of the computed *a priori* probability of occurrence of the event being predicted (e.g. exceeding a precipitation threshold).

The results obtained so far indicate that LEPS allows the combination of the benefits gained by a probabilistic approach with the high-resolution detail of LAM integrations, without having to pay too much in terms of computer power. It has been shown that, over a number of test cases and for forecast ranges between 48 and 120 hours, LEPS performs better than the standard EPS in estimating precipitation intensity and in detecting the regions most likely to be affected by heavy rain. These encouraging results have led to the experimental production of limited-area ensemble forecasts on a daily basis, as described in the next section.

The COSMO-LEPS project

The membership of COSMO (the COnsortium for Small-scale MOdelling), formed in October 1998, consists of the national meteorological services of Germany, Greece, Italy, Poland and Switzerland. Additionally, the regional weather service ARPA-SMR (Italy) and the military service AWGeophys (Germany) are participating in the project. The general goal of COSMO is to develop, improve and maintain a non-hydrostatic limited-area atmospheric model (Lokal Modell, LM) which is used both for operational and for research applications by the members of COSMO (see www.cosmo-model.org).

Following the encouraging results of LEPS experimentation at ARPA-SMR, the generation of limited-area ensemble forecasts has recently started within the COSMO framework. This project is aimed at the operational implementation of short-to-medium-range probabilistic forecasts (48–120 hours) of severe-weather events over a European domain (Figure 1) covering all countries involved in COSMO. An experimental operational COSMO-LEPS suite has been set up to produce real-time probabilistic forecasts based on the LM nested in a selection of ECMWF EPS members.

Suite implementation

A number of technical issues had to be faced during the implementation of the COSMO-LEPS suite.

- **CPU time constraints**: The clustering-selection technique at the basis of COSMO-LEPS methodology enables a considerable reduction in the number of LAM integrations that need to be performed compared with, for example, the 'brute force' approach. Thus, the COSMO-LEPS system is relatively cheap from a computational point of view. Nevertheless, it still requires the integration of a limited-area model (with a forecast length of 120 hours) five times a day. The five runs of the LM with the features described in the next section take approximately 403 hours of CPU time on ECMWF super-computers. Consequently, it would be extremely difficult for a single COSMO Member State to accomplish this task on its own on a daily basis without interfering heavily with the operational generation of routine meteorological forecasts.
- **Data transfer**: In order to set both the initial and the boundary conditions for the LM integrations from the analysis time to the final forecast time (120 hours later) every six hours, several meteorological fields need to be provided by the five selected EPS members and interpolated to the LM grid at all model levels (EPS members are run at T255L40 resolution). This would imply, every day, a data transfer of approximately 600 MB from ECMWF to the Member State running the COSMO-LEPS suite. This amount of data, although not so large by itself, would be a further burden added to the already intense 'traffic of data' between ECMWF and Member States. In addition to this, the COSMO-LEPS methodology would require dynamic selection of the fields to be disseminated (the forecast numbers of the five selected EPS members change from one day to another); this is not feasible with the present operational dissemination procedures.

Because of the above-mentioned technical problems (as well because of the assistance that could be provided by staff at ECMWF) the COSMO-LEPS suite has been implemented at ECMWF using the Supervisor Monitor Scheduler (SMS); an example of the COSMO-LEPS suite is shown in Figure 2. In order to nest the LM in EPS members, both the operational EPS suites (at 00 UTC and 12 UTC) had to be slightly modified so as to post-process the EPS output on the model levels and to include the calculation of some

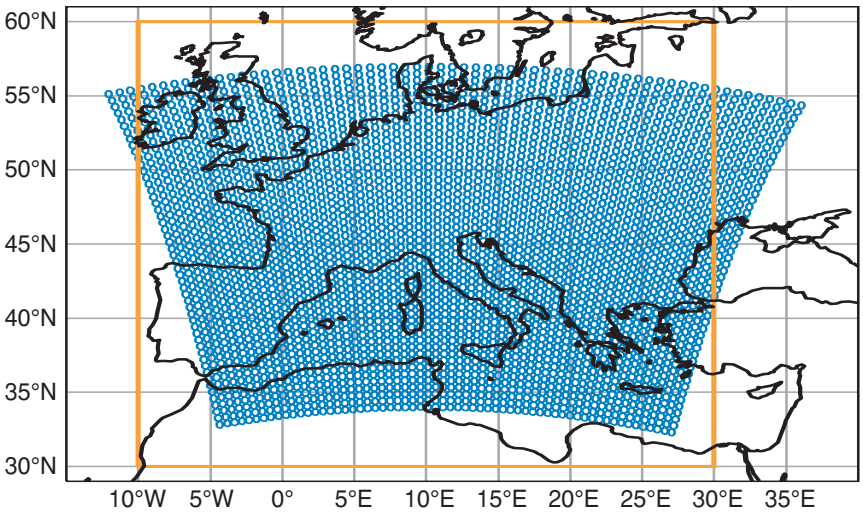

Figure 1 The COSMO-LEPS domain (blue dots) and the clustering domain (orange rectangle).

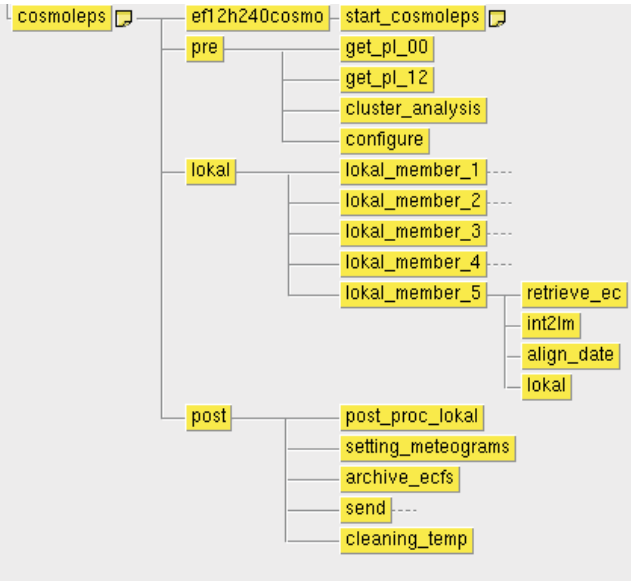

Figure 2 The COSMO-LEPS suite running under SMS at ECMWF.

extra surface parameters needed for the nesting. The computer resources needed by the COSMO-LEPS system (about 1600 billing units per day) are provided from allocations to the ECMWF COSMO partners (i.e. Germany, Greece, Italy and Switzerland), whose contributions were joined into a unique 'COSMO-account'.

Methodology

Thanks to the experience gained during the experimentation phase, it was decided to set up the suite as follows:

- Three successive 12-hour lagged EPS runs (started at 12 UTC of day D–1, and at 00 UTC and 12 UTC of day D) are grouped together so as to generate a 153-member super-ensemble; the three ensembles are referred to as the 'oldest', 'middle' and 'youngest' EPS, respectively (Figure 3);
- A hierarchical cluster analysis is performed on the 153 members so as to group all elements into five clusters (of different populations) – the 'complete-linkage' method is used to construct the clusters. The clustering variables are the geopotential height Z, the wind components (U,V) and the specific humidity Q at three pressure levels (500, 700, 850 hPa) and at two forecast times (fc+96h and fc+120h for the youngest EPS – corresponding to fc+108h and fc+132h for the middle EPS and to fc+120h and fc+144h for the oldest EPS[2]); the cluster domain covers the region 30°N–60°N, 10°W–30°E (slightly larger than the LM domain; see Figure 1);
- Within each cluster, one RM is selected according to the following criteria: the RM is the element closest to the members of its own clusters and most distant from the members of the other clusters. Distances are calculated using the same variables as for the cluster analysis; hence, five RMs are selected;
- Each RM provides both initial and boundary conditions for the integrations with the LM, which is run five times for 120 hours, from 12 UTC of day D to 12UTC of day D+5 (Figure 3);
- The LM domain covers central and southern Europe at a horizontal resolution of approximately 10 km (78948 grid points), with 32 vertical levels;
- Probability maps based on the LM runs (valid from day D+1 to day D+5) are generated by assigning to each LM integration a weight proportional to the population of the cluster from which the RM (providing initial and boundary conditions) was selected; deterministic products (that is, the five LM scenarios in terms of surface and upper-level fields) are also produced;
- The LM GRIB files are sent using ftp to the COSMO community.

As to product availability, the integration of the youngest EPS (started at 12 UTC of day D) is completed at ECMWF at about 00 UTC of day D+1. Therefore, since every 120-hour LM integration takes approximately 57 minutes (using 84 tasks), and three (or four) LM runs are performed at the same time, the COSMO-LEPS output is usually available by 05 UTC of day D+1, well in time to be used and evaluated by the bench forecasters of the COSMO meteorological services.

Product dissemination

At the time of writing (June 2003), the following fields are being post-processed and sent to the COSMO community:

Probabilistic products

- Probabilities of the 24-hour rainfall being above 20, 50, 100, 150mm;
- Probabilities of the 72-hour rainfall being above 50, 100, 150, 250mm;
- Probabilities of the 24-hour 2 m T_{max} being above 20, 30, 35, 40°C;
- Probabilities of the 24-hour 2 m T_{min} being below -10, -5, 0, +5°C;
- Probabilities of the 24-hour 10 m maximum wind being above 10, 15, 20, 25m/s;
- Probabilities of the 24-hour snow being above 1, 5, 10, 20mm of equivalent water;

Deterministic products (for each LM run)

- Rainfall and mean-sea-level pressure;
- Geopotential height at 700hPa and temperature at 850hPa;

Meteograms (over a number of station points)

- Precipitation;
- Surface temperature;
- Surface wind intensity.

In the near future, it is planned to enhance the present-day configuration, by adding the dissemination of other probabilistic fields, as well as of upper-level fields, for each of the five LM runs. At the moment, the ECMWF File Storage (ECFS) is being used for archiving the LM forecast fields. In the near future, it is planned to migrate the archiving to MARS, thus making the retrieval of LM integrations more 'user-friendly' and available to all Member States.

2 'fc+NNh' indicates a forecast range of NN hours since the beginning of the run; for example, 'fc+96h' means the 96-hour forecast range.

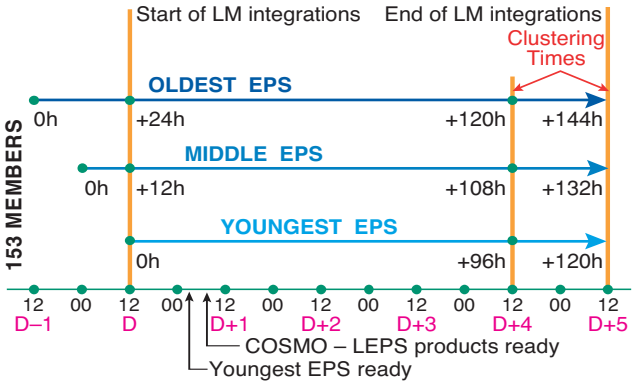

Figure 3 Details of the COSMO-LEPS methodology.

A heavy-precipitation event in northern Italy

As an example of COSMO-LEPS performance, we present the behaviour of the system for a heavy precipitation event that occurred in November 2002 in northern Italy. Figure 4 shows the observed precipitation values (accumulated over a 24-hour period ending at 12 UTC, 25 November 2002) in northern Italy. Rainfall values exceeding 100mm/day were recorded all over the southern Alpine area, the highest amounts being observed in north-eastern Italy (above 150mm/day). This caused widespread flooding as well as the overflow of several lakes.

To evaluate the behaviour of the COSMO-LEPS system, only products available in real time are presented and their usefulness assessed. Figure 5 shows the performance of the five LM forecasts (120-hour range) in terms of both the geopotential height at 700 hPa and the 24-hour accumulated precipitation. The first two LM integrations (Figures 5(a) and (b)) are quite accurate in terms of flow pattern when compared with the ECMWF verifying analysis (valid at 12 UTC 25 November 2002 and shown in Figure 5(f)). Both these integrations also predict high amounts of rainfall in the regions actually affected by heavy precipitation (as shown in Figure 4), although the quantitative precipitation is somewhat underestimated over north-eastern Italy. For reference, Figure 5(f) also shows the ECMWF 'rainfall analysis' (actually, a 24-hour forecast started at 12 UTC 24 November 2002). If compared directly with the observations of Figure 4, it can be noticed that the two precipitation patterns are similar, although the ECMWF 'rainfall analysis' underestimates the rainfall maxima in the Alpine area.

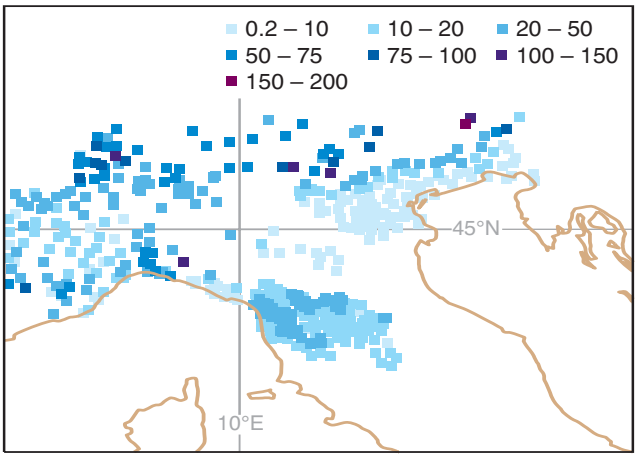

Figure 4 Observed precipitation over the 24-hour period ending at 12 UTC 25 November 2002 (observations obtained using the non-GTS network). The precipitation intensities are indicated in the colour key.

The south-westerly flow impinging on the Alps is not properly predicted in the third and fifth LM integrations (Figures 5(c) and (e)) since it is too much in the southern (eastern) direction in the former (latter) run. This causes a severe misplacement and underestimation of the predicted rainfall over northern Italy in both runs. The rainfall forecast is quite accurate in the fourth LM integration (Figure 5(d)) in terms of the detection of regions affected by heavy precipitation, although the circulation pattern is not accurately predicted. In summary, it is worth mentioning that, already at the longest forecast range (120 hours), three (out of five) LM integrations produce accurate forecasts in terms of precipitation, thereby providing the possibility of issuing preliminary warnings to be either confirmed or dismissed on the basis of more recent forecasts.

In addition to the five LM deterministic runs, a further (and probably the main) COSMO-LEPS product consists in combining these five runs using weights proportional to the population of the clusters in which the RMs providing initial and boundary conditions were selected (for clarity, the populations of the clusters are shown above the panels in Figure 5). This enables the generation of probability maps on the basis of the LM forecasts. For this case study, Figure 6 shows the probability forecast (120-hour range) of one-day rainfall exceeding four different thresholds: 20, 50, 100 and 150 mm. For the two lowest thresholds (Figures 6(a) and (b)), all regions actually affected by the flooding are highlighted as locations of heavy rainfall, with probabilities above 90% over north-western Italy for the 20 mm threshold. At the two highest thresholds (Figures 6(c) and (d)), only the signal over north-western Italy 'survives', with a probability of rainfall greater than 150 mm being between 30% and 60%.

It is also possible to assess in real time the consistency of the COSMO-LEPS probability forecasts. For this case study, the behaviour of the system is evaluated for four different prediction ranges (fc+120, fc+96, fc+72 and fc+48h) and attention is focused on the probabilistic forecast of 24-hour rainfall exceeding 100 mm. At the longest forecast range (Figure 7(a) – the same as Figure 6(c)), it can be noticed that the possibility of a heavy-precipitation event is already highlighted in north-western Italy with a probability above 30%. As the range gets shorter (Figures 7(b) and (c)), large parts of northern Italy are shown as possible locations of heavy rainfall (as actually happened), the probability values becoming higher as the forecast range is reduced. At the shortest range (Figure 7(d)), the rainfall probability exceeds 90% over Piedmont and Liguria as well as over parts of north-eastern Italy. Hence, as the forecast range decreases the flood scenario becomes more likely, thus providing the possibility of issuing early flood warnings and alerting those governmental bodies responsible for civil protection.

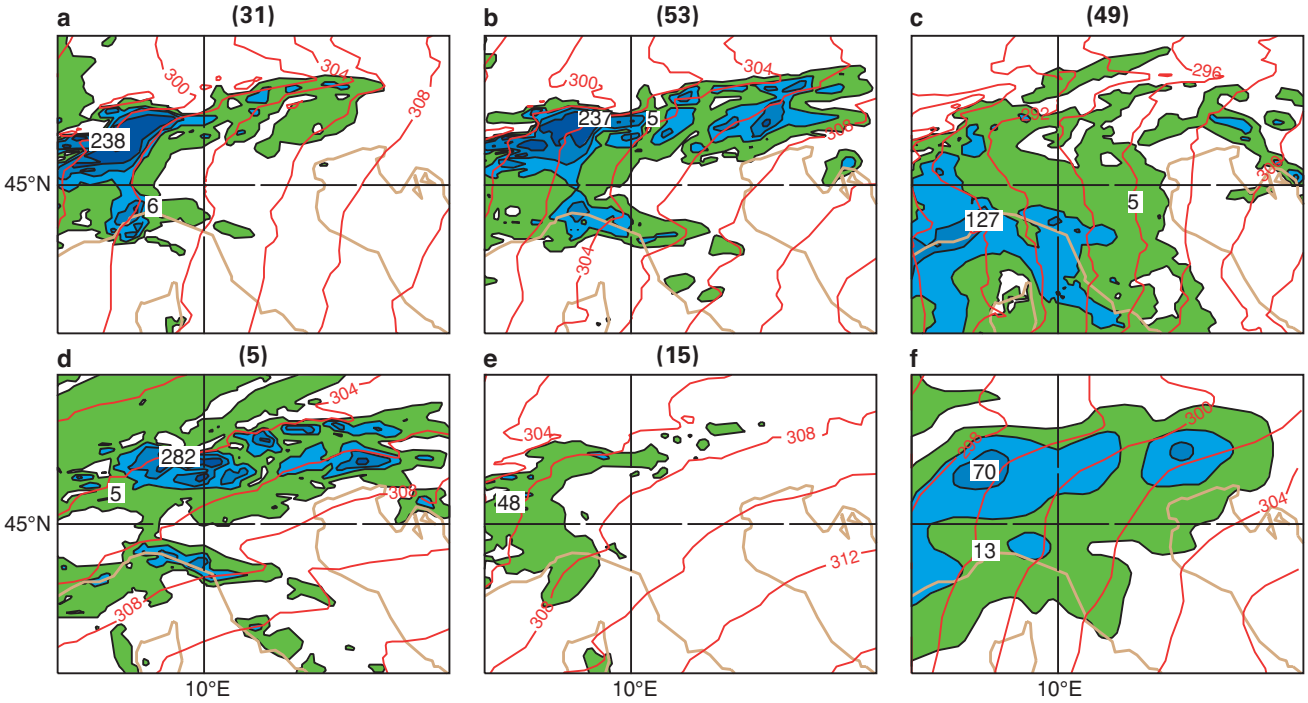

Figure 5 (a), (b), (c), (d), and (e) The 120-hour forecast geopotential height at 700 hPa (red lines) and 24-hour precipitation (accumulated between fc+96h and fc+120h, filled areas) for the five individual COSMO-LEPS deterministic integrations starting at 12 UTC 20 November 2002. The cluster population is also indicated above each panel. (f) The ECMWF analysis in terms of geopotential height at 700 hPa (valid at 12 UTC 25 November 2002) and the 24-hour precipitation (accumulated from 12 UTC 24 November to 12 UTC 25 November 2003). The contour intervals are 20 dam for 700 hPa geopotential height, and 2, 20, 50, 100, 200 and 500mm for precipitation.

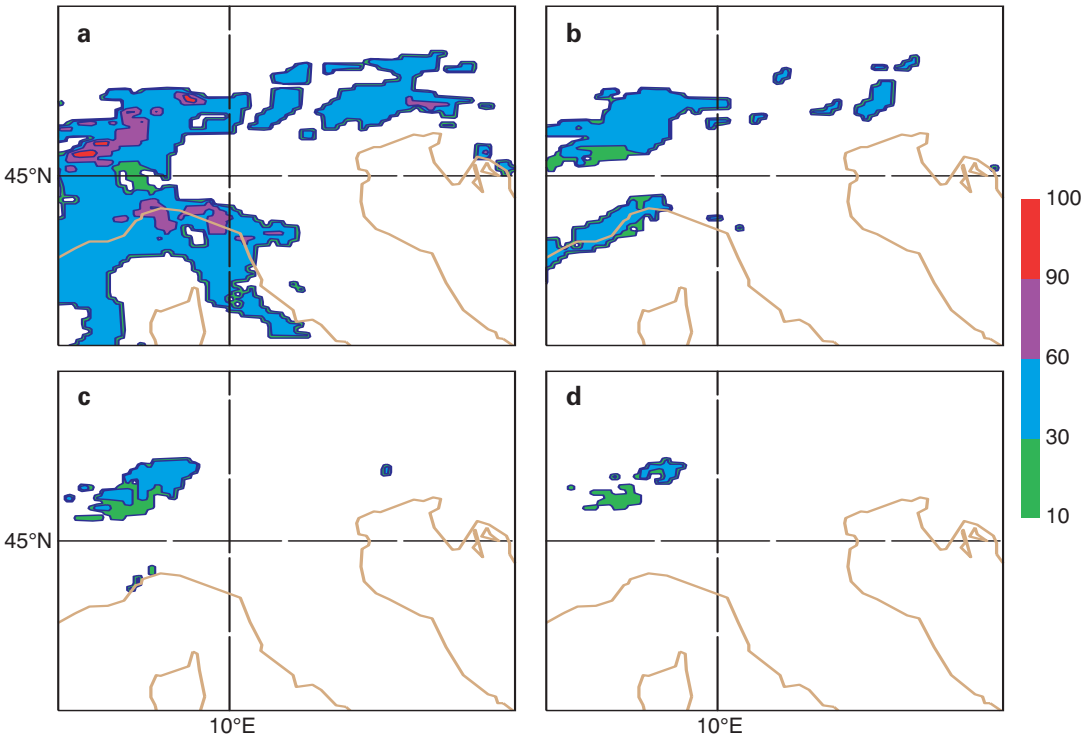

Figure 6 Maps of the probability of the 24-hour rainfall exceeding (a) 20 mm, (b) 50 mm, (c) 100 mm, and (d) 150 mm for the COSMO-LEPS 120-hour runs starting at 12 UTC 20 November 2002. The contour intervals are 10%, 30%, 60% and 90%.

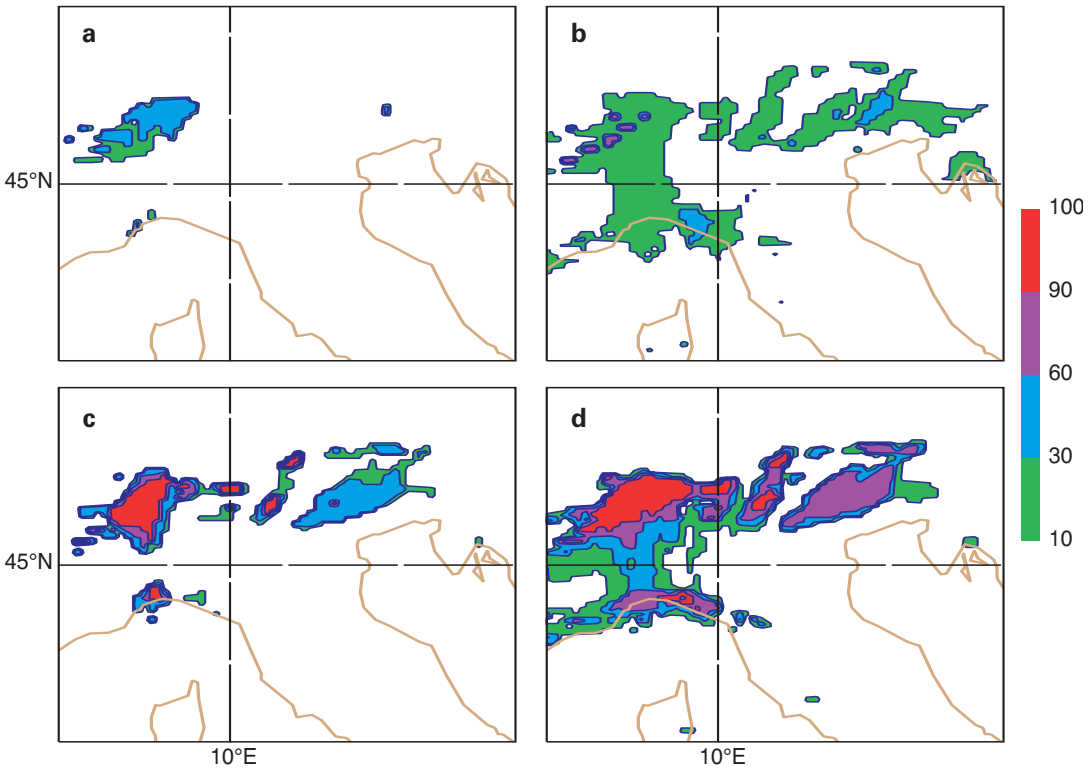

Figure 7 The COSMO-LEPS maps of the probability of the 24-hour rainfall exceeding 100 mm for the forecasts starting at (a) 12 UTC 20 November 2002 (120-hour range), (b) 12 UTC 21 November 2002 (96-hour range), (c) 12 UTC 22 November 2002 (72-hour range), and (d) 12 UTC 23 November 2002 (48-hour range). All maps are valid at 12 UTC 25 November 2002. The contour intervals are 10%, 30%, 60% and 90%.

Future developments

After three years of tests over a number of cases with very satisfactory results, an experimental operational phase of the COSMO-LEPS project started in November 2002. Deterministic and probability products based on the Lokal Modell are generated on a daily basis and are disseminated to the meteorological services taking part in the COSMO consortium. The test suite is running at ECMWF without interfering with the operational duties of the Centre and is being monitored and controlled remotely by ARPA-SMR.

The performance of the system for detecting the regions most likely to be affected by intense and localised rainfall events, as well as for estimating the precipitation quantitatively, seems to be promising. During the first year of activity of the system, it is planned to test its usefulness and skill. In particular, the assistance given to forecasters in cases of extreme events will be assessed and the forecast accuracy of COSMO-LEPS products will be examined on the basis of several objective scores; this should enable an evaluation of both the capability and shortcomings of the COSMO-LEPS system in a comprehensive way. These tests will provide a good basis for assessing the usefulness of the COSMO-LEPS system in providing forecasts of intense meteorological events in the short-to-medium range. Finally, a modification of the present-day configuration to include not only uncertainties coming from different initial and boundary conditions, but also model uncertainties, will also be tested. It is also planned to assess the impact of using different convection schemes, although other options will be explored too.

Acknowledgements

The authors acknowledge the support and encouragement of Franco Molteni (ICTP) and Roberto Buizza (ECMWF) in the early stages of this work. We are also grateful to Carlo Cacciamani (ARPA-SMR) for useful discussions. Finally, the cooperation and special efforts provided by ECMWF for the full implementation of the project has to be explicitly praised.

Further reading

Marsigli, C., **Montana, A.**, **Nervosa, F.**, **Paccagnella, T.**, **Tibaldi, S.**, **Molteni, F.** and **Buizza, R.**, 2001: A strategy for high-resolution ensemble prediction. II: Limited-area experiments on four Alpine flood events. *Q.J.R. Meteorol. Soc.*, **127**, 2095-2115

Molteni, F., **Buizza, R.**, **Marsigli, C.**, **Montani, A.**, **Nerozzi, F.** and **Paccagnella, T.**, 2001: A strategy for high-resolution ensemble prediction. I: Definition of representative members and global-model experiments. *Q.J.R. Meteorol. Soc.*, **127**, 2069-2094

A. Montani[1], *M. Capaldo*[2], *D. Cesari*[1], *C. Marsigli*[1], *U. Modigliani*[3], *F. Nerozzi*[1], *T. Paccagnella*[1], *P. Patruno*[1] *and S. Tibaldi*[1]
[1] Regional Meteorological Service ARPA-SMR, Italy, [2] Ufficio Generale Meteorologia, Italy, [3] ECMWF

Forecasts of severe convection

Forecasting severe convection is a difficult area as typical convective systems consist of one or multiple convective draughts having lifetimes of the order of one hour that interact with their environment. Furthermore, local features like orography may significantly influence the formation / propagation of convective systems. However, intense convective systems are generally associated with synoptic disturbances, like midlatitude frontal systems or tropical waves, that provide the necessary destabilization of the atmosphere as expressed by the CAPE (Convective Available Potential Energy). Once the region near cloud base that generally forms a potential barrier to moist convection becomes unstable by large-scale lifting or turbulent processes, the CAPE can be released in convective towers by condensational heating (through the formation of precipitation) and is consequently converted into kinetic energy of the strong ascending/descending motions.

A forecast model may struggle to forecast correctly the timing and location of convection and the total rainfall as these features depend essentially on the quality of the model's convection parametrization, the quality of the analysis (especially the humidity analysis), and the horizontal resolution of the model. However, the synoptic environment favourable for convective development (such as low-level warm-air advection, lifting of the atmosphere, and upper-level divergence in the vicinity of the jet stream) are generally reasonably well predicted by the forecast model up to several days in advance. With a quality medium-range forecast model, an experienced forecaster may, therefore, be able to identify potential areas of convective activity on the basis of synoptic maps (including, for example, CAPE and vertical soundings), whereas satellite and radar imagery are able to support short-range forecasting and nowcasting.

The aim of the present article is to discuss the ability of the ECMWF Integrated Forecasting System (IFS) to forecast severe continental convection on the basis of two recent cases:

1 a flash-flood event that occurred in southern France on 9 September 2002 associated with precipitation amounts exceeding 600 mm in 48 hours (causing 22 casualties), and
2 a tornado outbreak that occurred in the central USA on 4–5 May 2003, with more than 80 tornadoes forming in mesoscale convective systems (killing 40 people).

Of particular interest is the sensitivity of the forecasts to the model's convection parametrization, which has recently undergone important changes.

Convection parametrization

With deep (shallow) convective motions having typical horizontal scales of 10^3m (10^2m), the ensemble-mean effect of convective draughts must be parametrized in the IFS T511 (40 km horizontal resolution) deterministic forecast. However, convective motions are often embedded within mesoscale convective or frontal systems that are explicitly resolved by the model. Therefore, cloud mass is exchanged in the model between the parametrized convection and the resolved dynamics/microphysics.

Briefly, the IFS computes convective precipitation and convective adjustment (stabilization) of the atmosphere with the aid of a mass-flux scheme (*Tiedtke* 1989; *Gregory et al.* 2000). The scheme consists of three parts:

1 a process where (for each model column) the convectively unstable layers, the cloud-base properties, and the type of convection (shallow, deep, mid-level) are determined, followed by
2 a cloud scheme that computes the properties of one representative convective cloud, and
3 a closure that determines the absolute value of the convective precipitation and mass flux (the updraught vertical velocity times the updraught area) as being proportional to the CAPE, as well as the final convective tendencies.

In cycle 25r1 of the IFS (operational until 13 January 2003), deep convection was only allowed to be initiated from the first model level above the surface. As a consequence, the model underestimated the convective adjustment and precipitation in the presence of a stable surface layer (e.g. over land during the night), and also generally underestimated it when the convection originated from elevated unstable layers. In cycle 25r4 (currently operational), this problem was addressed by computing parcel ascents from model layers in the lowest 700 hPa of the atmosphere, and retaining the first ascent (from the bottom) that produces a sufficiently deep cloud. Further modifications included the parcel's initial temperature and moisture perturbations, and adjustments to the cloud parameters of the scheme.

In the first of the following two case studies the deterministic forecast using the forecast scheme in cycle 25r1 is compared with the results from cycle 25r4 (run experimentally). The second case has been run exclusively with cycle 25r4, which was already operational at that time. The focus is on forecast consistency and the predictability of strongly forced convection in the light of the model's convective adjustment process. Features, such as the vertical wind profiles and mid-level dry layers, which have an important impact on the nature of convection, are also discussed.

The 9 September 2002 flash flood in southern France (Gard)

Between late summer and winter the Mediterranean basin is frequently subjected to severe weather, such as heavy rainfall and severe winds. Rainfall events of over 200 mm and, in some cases, in excess of 600 mm in 24 hours, have been known to occur from time to time, while sustained wind speeds in excess of 100 km/h are often associated with low-level cyclones or local orographic features. Recent devastating events have been documented by, for example, *Sénési et al.* (1996) and *Bechtold and Bazile* (2001), and the Mesoscale Alpine Programme (MAP) in 1999 has been especially devoted to the investigation of intense precipitation events over orography.

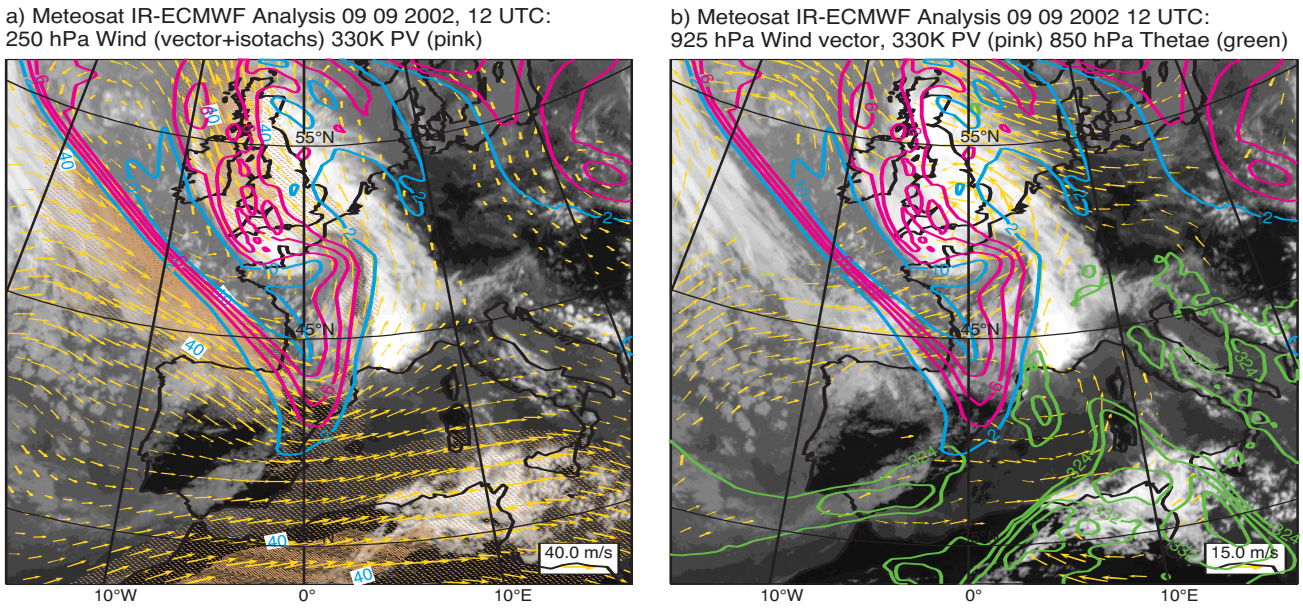

Figure 1 The Meteosat infrared image for 12 UTC 9 September 2002 together with the ECMWF analysed values of (a) the 330 K potential vorticity (pink and blue isolines), and the 250 hPa wind vectors (arrows) and isotachs (dotted brown areas), and (b) the 330 K potential vorticity, the 925 hPa wind vectors (arrows), and the 850 hPa equivalent potential temperatures (green isolines). The equivalent-potential-temperature contours are incremented by 4 K starting with a value of 324 K, and the PV increments are 2 PVU (potential vorticity units). The unit length for the wind vector is 40 m/s in (a) and 15 m/s in (b).

The present event occurred between 8 and 9 September 2002 when rain accumulations in excess of 600 mm in 48 hours were observed in southern France. A detailed description of the event is given on the Web site of Météo-France[1].

Figure 1 displays the Meteosat infrared satellite image at 12 UTC 9 September 2002 together with the ECMWF analysis. Convective systems are conveniently characterized by upper and lower-tropospheric charts, as represented here by the potential vorticity (PV) on the 330 K potential temperature surface, and the 250 hPa wind field (Figure 1(a)), as well as by the 330 K PV, the 925 hPa wind field and the 850 hPa equivalent potential temperature (Figure 1(b)). The reader might be more familiar with looking at geopotential maps on constant pressure surfaces instead of PV maps on constant potential-temperature surfaces. The two approaches are equivalent; PV maps, however, show more structure than the geopotential maps.

This is a textbook example of explosive convective development. A V-shaped convective system forms over the French Mediterranean coast in a large-scale environment characterized by upper-level divergence in the left-exit region of the jet, and low-level convergent flow of warm and moist air from the Mediterranean (high values of equivalent potential temperature) that is partly reinforced by local orographic effects. The maximum analysed upper-level wind speed attains values of 50 m/s at the western side of the PV anomaly, but the maximum upper-level and low-level wind speeds in the vicinity of the convective system are about 30 m/s and 10 m/s, respectively. The convective system forms under the south-east side of the upper-level PV anomaly that corresponds to the cyclonic-shear side of the flow; such narrow meridionally elongated PV anomalies are also called PV streamers. Note also that the PV anomaly marks a region with a low tropopause and a relatively cold and unstable troposphere.

The results from the 48-hour forecasts with cycles 25r1 and 25r4 starting at 12 UTC 7 September 2002 are depicted in Figure 2. The two forecasts are in close agreement, but the low-level equivalent-potential-temperature field of the 25r4 forecast fits the corresponding analysis (Figure 2(b)) slightly better. Nevertheless, both forecasts underestimate the deepening of the main depression over Northern France and Southern England.

Up to now, only the lower and upper troposphere has been considered. However, the presence of mid-level dry layers is also of interest for forecasters as such layers might suppress convective activity, but also favour the formation of intense convective downdraughts that might lead to strong surface wind gusts. A zoom on the analysed 700 hPa wind and equivalent potential temperature field at 12 UTC is presented in Figure 3. In the convective region one can distinguish two maxima of equivalent potential temperature that are separated by a dry region. The consequences and evolution of these dry layers are further discussed in the next section.

Convective instability, adjustment and precipitation

Convective adjustment is a fast process that implies a subtle balance between the large-scale dynamic tendencies and the parametrized convective tendencies; either of the tendency terms might be as large as 100 K/day. Problems

1 http://www.meteo.fr/meteonet/actu/archives/evenements/Nimes/eve.htm

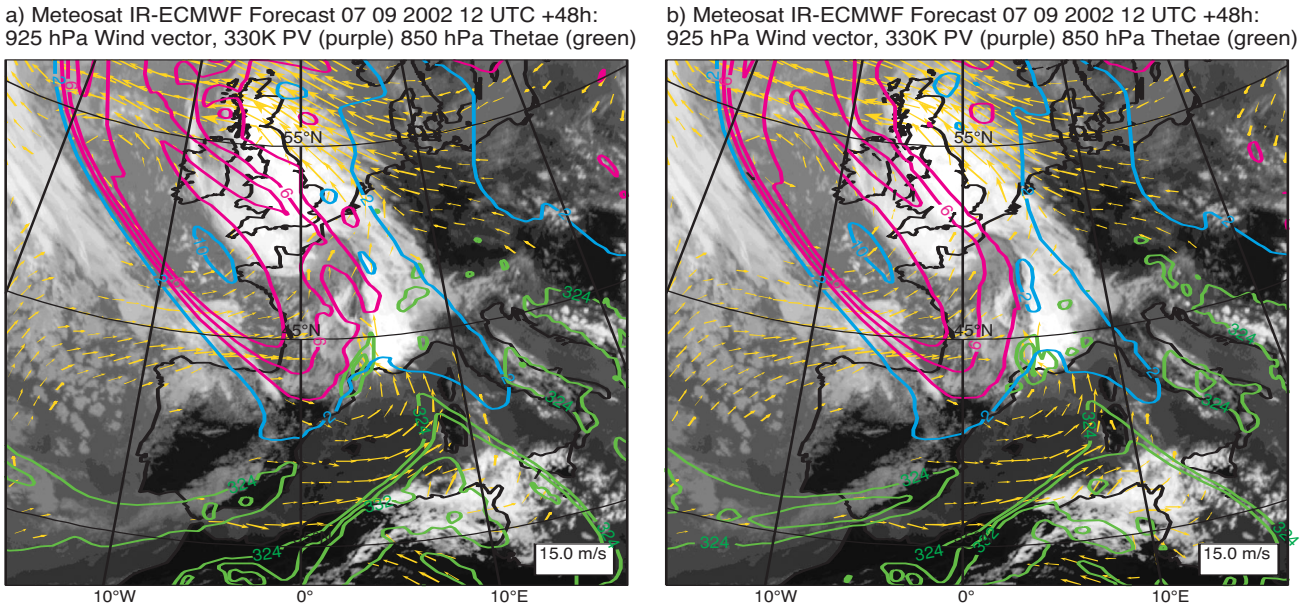

Figure 2 As Figure 1(b), but from 48-hour forecasts starting at 12 UTC 7 September 2002 (a) using cycle 25R1, and (b) using cycle 25r4.

in the model's convection parametrization might, therefore, significantly affect the forecast profiles during the convective adjustment process. To illustrate the convective adjustment process in the model, the forecast soundings with cycle 25R4 and analysed soundings at 12 UTC and 18 UTC for the point (44°N, 5°E), affected by the convective system, are depicted in Figure 4. In the forecast (Figure 4(a)), the convectively unstable 12 UTC sounding experiences (during the following six hours) upper-tropospheric (lower-stratospheric) cooling (warming) of about 1-2 K, associated with the passage of the upper-level disturbance and with strong boundary-layer cooling of more than 5 K due to the evaporation of rain in the (parametrized) convective downdraughts (note the dry layer between 700 and 500 hPa at 12 UTC). Generally, the forecast soundings closely fit the analysed soundings. However, during this fast adjustment process, the 18 UTC forecast 600–700 hPa humidity values are drier than the corresponding analysis - compared with temperature and momentum, the convective transport/adjustment of moisture is more difficult to represent as it is only weakly constrained dynamically.

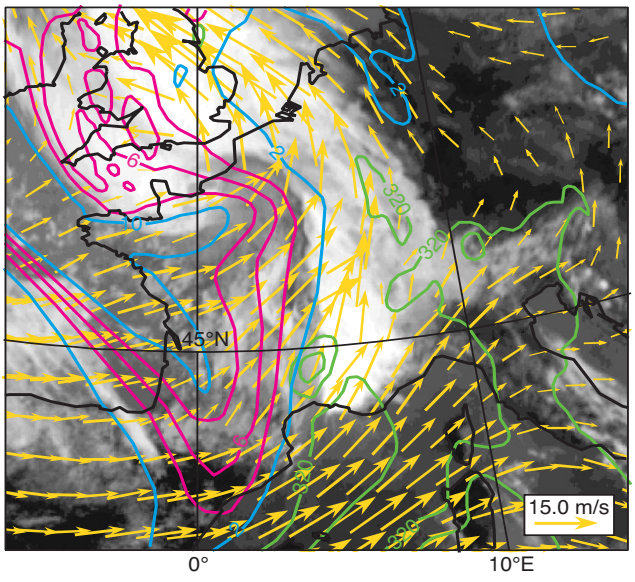

Figure 3 As Figure 1(b), but for a zoom showing the analysed 330 K potential vorticity, 700 hPa wind, and 700 hPa equivalent potential temperature (green isolines) for 12 UTC 9 September 2002. Note the pattern of dry and moist regions in the vicinity of the convective system.

The potential convective instability of the atmosphere is best represented by the CAPE. Its distribution for 00 and 12 UTC 9 September is plotted in Figure 5 as computed from two forecasts with cycle 25r4 starting, respectively, from 12 UTC 7 and 12 UTC 8 September. The two forecasts are reasonably consistent, as both show a very localized CAPE distribution, with maxima between 1500 and 2000 J/kg occurring at 00 UTC over the sea (in agreement with radar-derived precipitation rates, not shown) and at 12 UTC next to the French Mediterranean coastline. Therefore, the forecasts contain the necessary synoptic meteorological information to provide a precipitation forecast that is at least accurate in position. The high-density rain-gauge observations (Figure 6(c)) upscaled to the model's grid resolution show 24-hour rainfall amounts between 06 UTC 9 September and 06 UTC 10 September of 20–50 mm over Great Britain that are associated with the main frontal system, as well as a region with rainfall amounts exceeding 100 mm over south-central France that was affected by the convective system and a third precipitation zone over Germany and the Benelux. However, the 25r1 forecast (Figure 6(a)) had problems in representing the precipitation in the vicinity of the French Mediterranean coast and over Germany and, on the other hand, produced some spurious

high precipitation amounts over central and western France. As most of the forecast precipitation was of the stratiform type, the model produced insufficient convective adjustment (stabilization) of the atmosphere at the southeast side of the upper-level PV anomaly. This area of instability was then transported downstream, leading to spurious rainfall. With cycle 25r4 the rainfall over southern France was mainly of the convective type and the rainfall distribution was significantly improved over most parts of the domain (Figure 6(b)), even if the absolute values were still underestimated over southern France. However, this might also be related to insufficient model horizontal resolution (lack of orographic details and upslope flow) or to an inflow region that is initially too dry.

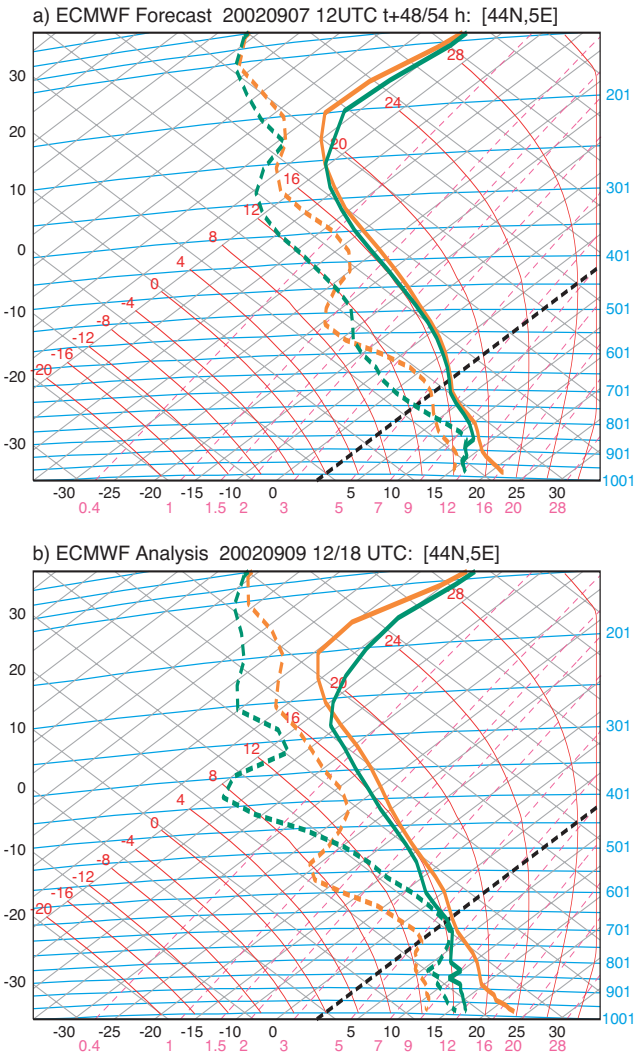

Figure 4 Tephigrams of (a) the 48-hour (red) and 54-hour (green) forecast soundings, and (b) the analysed soundings for 12 UTC (red) and 18 UTC (green) 9 September 2002. The starting time of the 25r4 forecast is 12 UTC 7 September 2002. Note the strong cooling below 700 hPa between 12 and 18 UTC due to the evaporation of rain and the lowering of the tropopause that is associated with the passage of the upper-level disturbance.

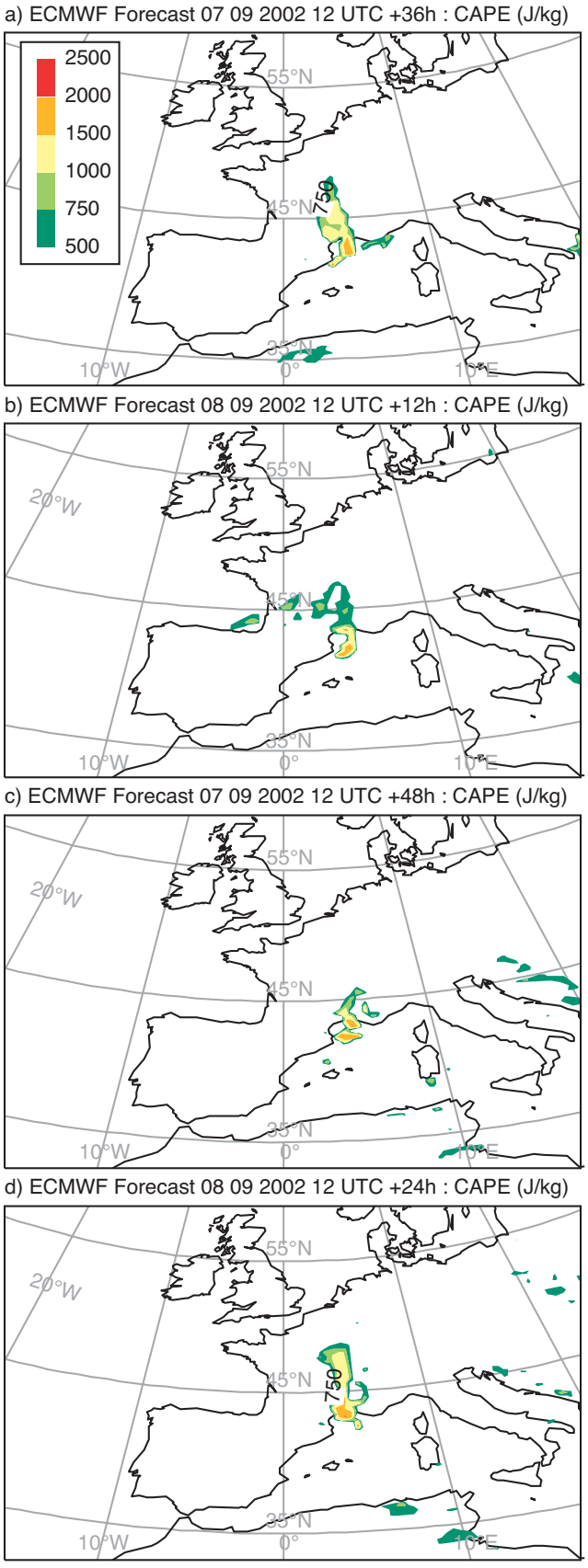

Figure 5 The CAPE (J/kg) over Western Europe (a) and (b) for 00 UTC 9 September, and (c) and (d) for 12 UTC 9 September from two forecasts with cycle 25R4 starting (a) and (c) at 12 UTC 7 September, and (b) and (d) at 12 UTC 8 September.

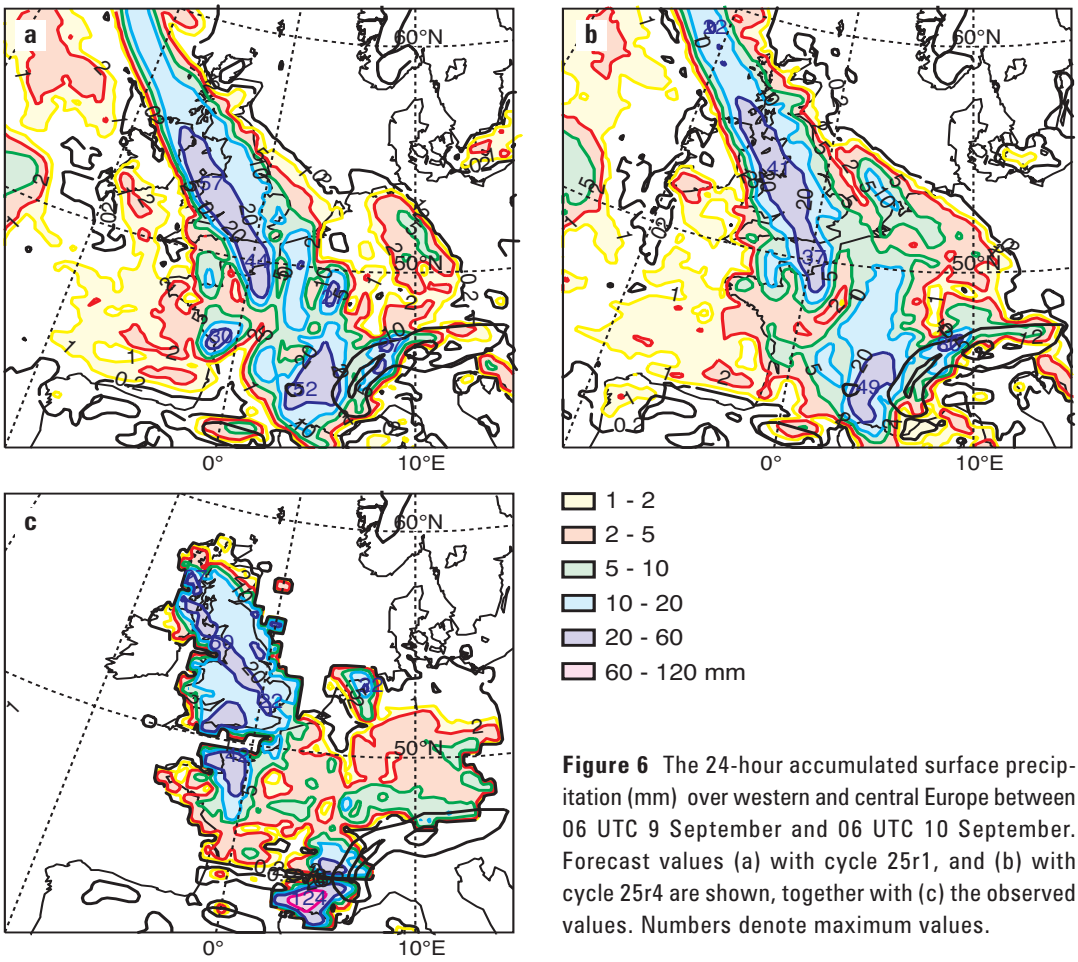

Figure 6 The 24-hour accumulated surface precipitation (mm) over western and central Europe between 06 UTC 9 September and 06 UTC 10 September. Forecast values (a) with cycle 25r1, and (b) with cycle 25r4 are shown, together with (c) the observed values. Numbers denote maximum values.

The 4–5 May 2003 tornado outbreak in the central USA

Intense mesoscale convective systems are particularly prominent over the Great Plains of North America during the spring convective season when synoptic systems transport warm and moist air from the Gulf of Mexico northwards where these air masses encounter upper-level cold anomalies. The strong convective updraughts in these systems sometimes result in the formation of tornadoes. A severe convective outbreak occurred on 4–5 May 2003 with more than 80 tornado touchdowns recorded (killing 40 people), and severe convective activity persisted with a total of 400 tornadoes recorded in the week between 4 and 10 May (source NOAA National Weather Service). This was the most intense convection outbreak since 3–5 May 1999.

Synoptic maps and wind shear

The GOES satellite imagery for 00 UTC 5 May 2003 (Figure 7) shows a series of convective clusters along 90°W that formed ahead of the upper-level PV anomaly in a region with strong upper-level divergent flow and strong low-level inflow of warm and moist air. Interestingly, the large divergence area corresponds to the exit region of two jet streaks, one located at the southern side of the PV anomaly 'in phase' with the anomaly, and the principal jet streak associated to the subtropical jet that was located at around 34°N and crossed the low-level flow near 88°W. There was also some weaker convective activity in the region spanned by the upper-level PV anomaly. Though the synoptic situation strongly resembled the European case discussed previously, there was a large difference in scale. The maximum upper- and lower-level wind speeds attained values of 65 m/s and 25 m/s, respectively, in the convective region, and the PV anomaly had a horizontal scale of roughly 2000 km (the scales of the PV anomaly and wind speeds are related). These values are about a factor of two larger than the values for the European case. Furthermore, the vertical wind shear (the change of the horizontal wind vector with height) attained particularly high values of about $8 \times 10^{-3} s^{-1}$ (65 m/s over 8 km). Vertical wind shear has a particular effect on the evolution of convective systems in that it makes the occurrence of convection more difficult as it inclines the convective draughts. However, once penetrative updraughts are formed it can make them more long-lived and adds rotation to the system through the so-called 'tilting' term in the vorticity equation. As a result, the potential for severe convection is often expressed by a bulk Richardson number obtained as the ratio of CAPE to the square of the overall vertical wind-shear vector.

Another interesting feature of the present case is the presence of a tongue of dry air at 700 hPa in the convective region, which favours the formation of convective downdraughts and surface gusts. It can be distinguished in Figure 8 as the region between two maxima of equivalent potential temperature marking the pre-convective environment and the post-convective inflow region, respectively.

a) GOES IR-ECMWF Analysis 05 05 2003 0 UTC:
250 hPa Wind (vector+isotachs), 330K PV (purple)

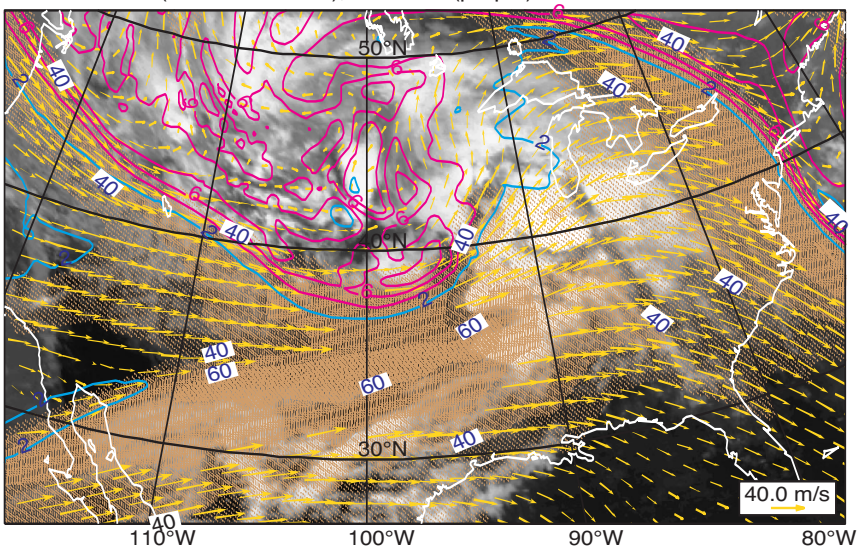

b) GOES IR-ECMWF Analysis 20030505 0 UTC:
925 hPa Wind vector, 330K PV (purple) 850 hPa Thetae (green)

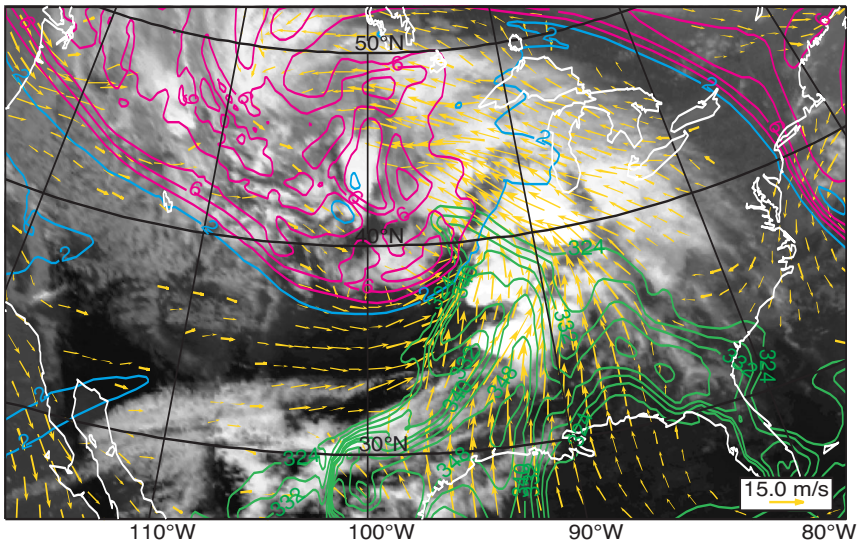

Figure 7 The GOES infrared image for 00 UTC 5 May 2003 together with ECMWF analysed values (a) of the 330 K potential vorticity (pink and blue isolines), and the 250 hPa wind vectors (arrows) and isotachs (dotted brown areas), and (b) the 330 K potential vorticity, the 925 hPa wind vectors (arrows), and the 850 hPa equivalent potential temperatures (green isolines). The equivalent-potential-temperature contours are incremented by 4 K, starting with a value of 324 K, and the PV increments are 2 PVU. The unit length for the wind vector is 40 m/s in (a) and 15 m/s in (b).

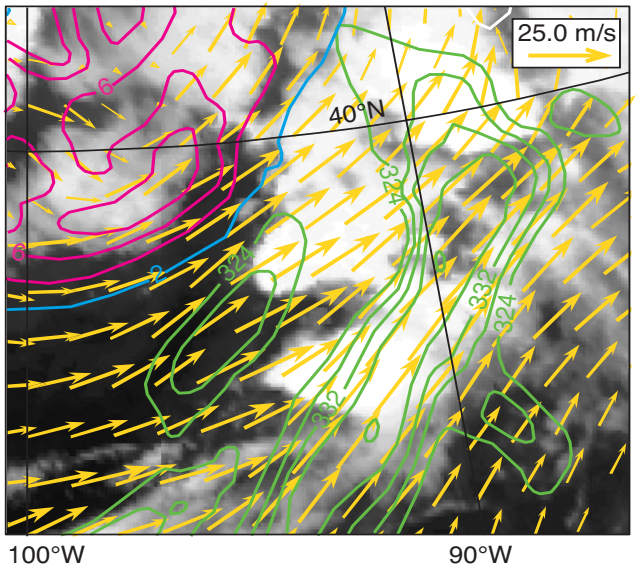

Figure 8 As Figure 7(b), but for a zoom showing the analysed 330 K potential vorticity, 700 hPa winds, and 700 hPa equivalent potential temperatures (green isolines) for 00 UTC 5 May 2003. The unit length for the wind vector is 25 m/s. Note the pre-convective region of warm/moist air that is followed by a dry tongue (no isolines) and a post-convective moist region.

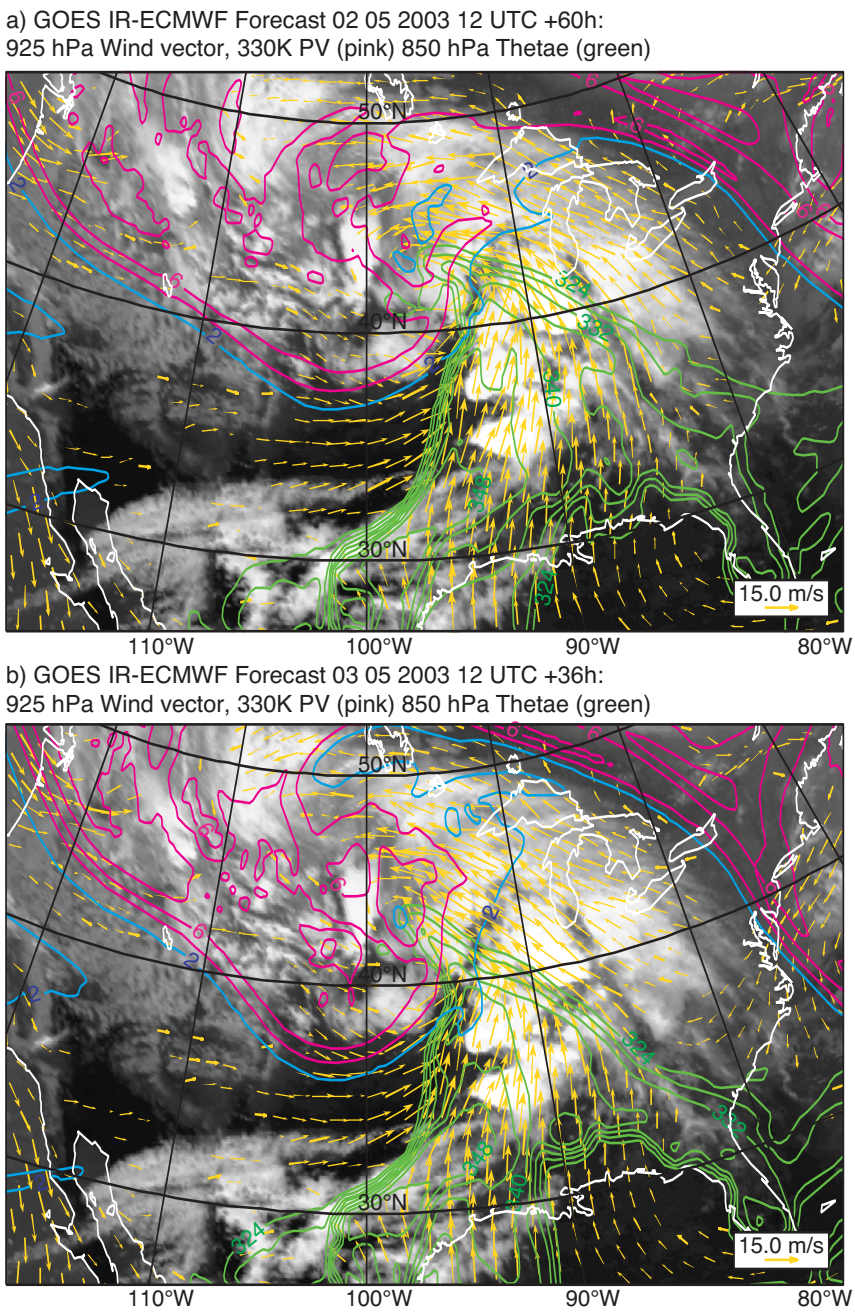

Figure 9 As Figure 7(b), but for (a) the 60-hour operational forecast (cycle 25R4) starting at 00 UTC 2 May 2003, and (b) the 36-hour operational forecast starting 12 UTC 3 May.

The operational (cycle 25r4) forecasts (Figures 9(a) and (b)) reproduced well the synoptic flow at least 60 hours in advance. The main difference between the 60-hour and 36-hour forecasts, both verifying at the same time, is a shift to the northeast of the low-level warm/moist sector. The analysed and forecast profiles in the convective region (not shown) evolved in a manner very similar to those shown in Figure 4, i.e. the atmosphere is destabilized by the action of low-level moist and warm advection and upper-level cold advection. Convection then stabilizes the atmosphere, mainly through cooling in the levels below 700 hPa; this attained maximum values of 10 K in six hours, compared with 5 K in six hours in the European case. The mid- and upper-troposphere, however, remained in a state that was close to moist adiabatic because strong large-scale cooling opposed strong convective warming.

CAPE and precipitation

A comparison of the CAPE values for 12 UTC 4 May and 00 UTC 5 May produced by the forecasts starting at 12 UTC 2 May and 12 UTC 3 May, is illustrated in Figure 10. Similar comments to those for the comparison of the synoptic fields in Figure 9 apply. Both the 60-hour and the 36-hour forecasts, verifying at the same time, produced high values of CAPE (up to 4000 J/kg, compared with maximum values of 2000 J/kg for the European case) in a rectangle between 88°W and 100°W, centred at 38°N, the region where tornadoes were actually reported. Nevertheless, high CAPE values do not necessarily correspond to observed convective activity that might be suppressed by a capping inversion (typically between 950 and 800 hPa) – the high CAPE values south of 34°N in Figures 10 (c) and (d) did not correspond to significant convective activity on the satellite image (Figure 7).

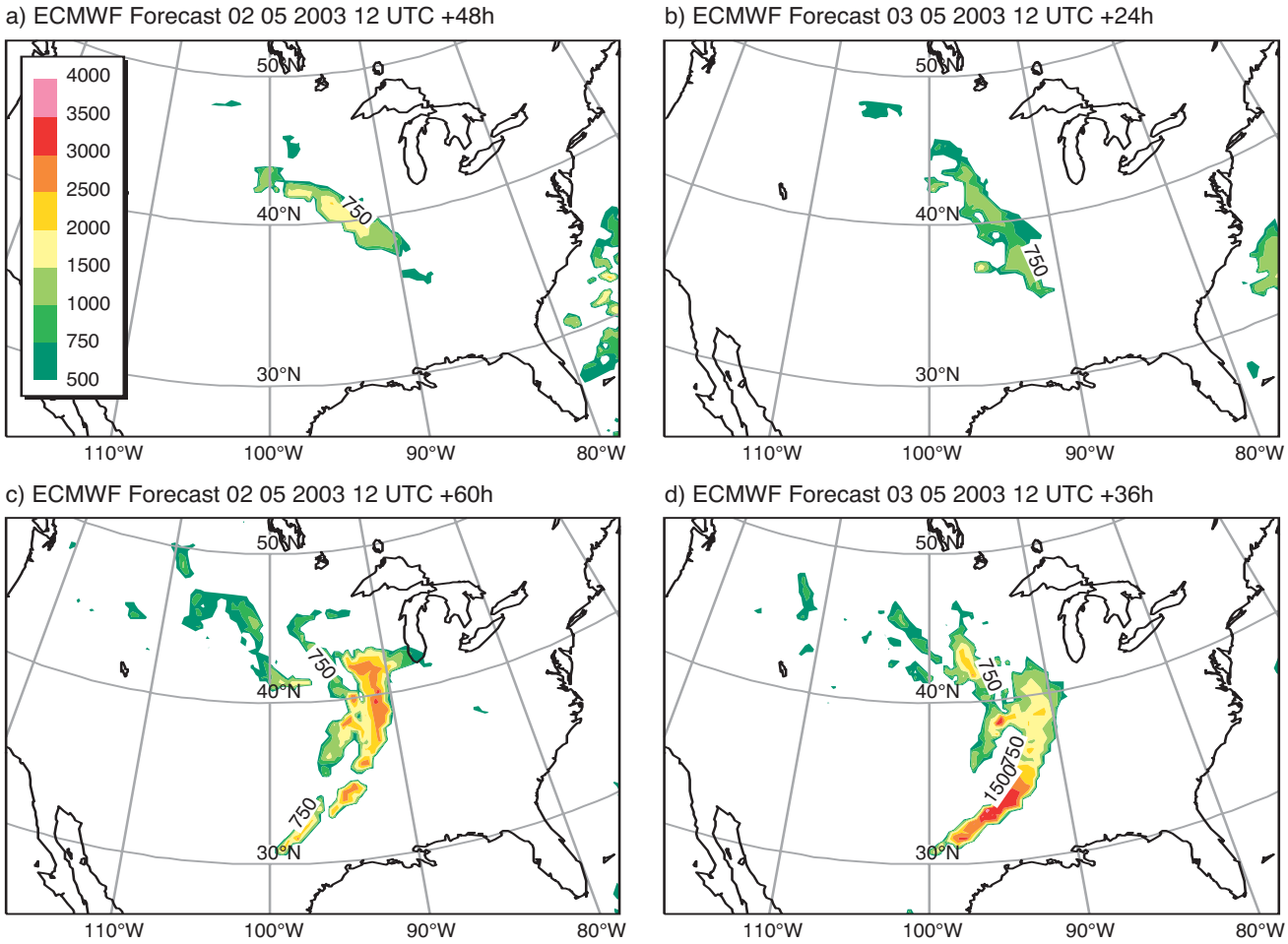

Figure 10 The CAPE (J/kg) (a) and (b) for 12 UTC 4 May 2003, and (c) and (d) for 00 UTC 5 May from cycle 25R4 forecasts starting (a) and (c) at 12 UTC 2 May, and (b) and (d) at 12 UTC 3 May. Colour intervals are 250, 500, 750, 1000, 1500, 2000 etc. (J/kg).

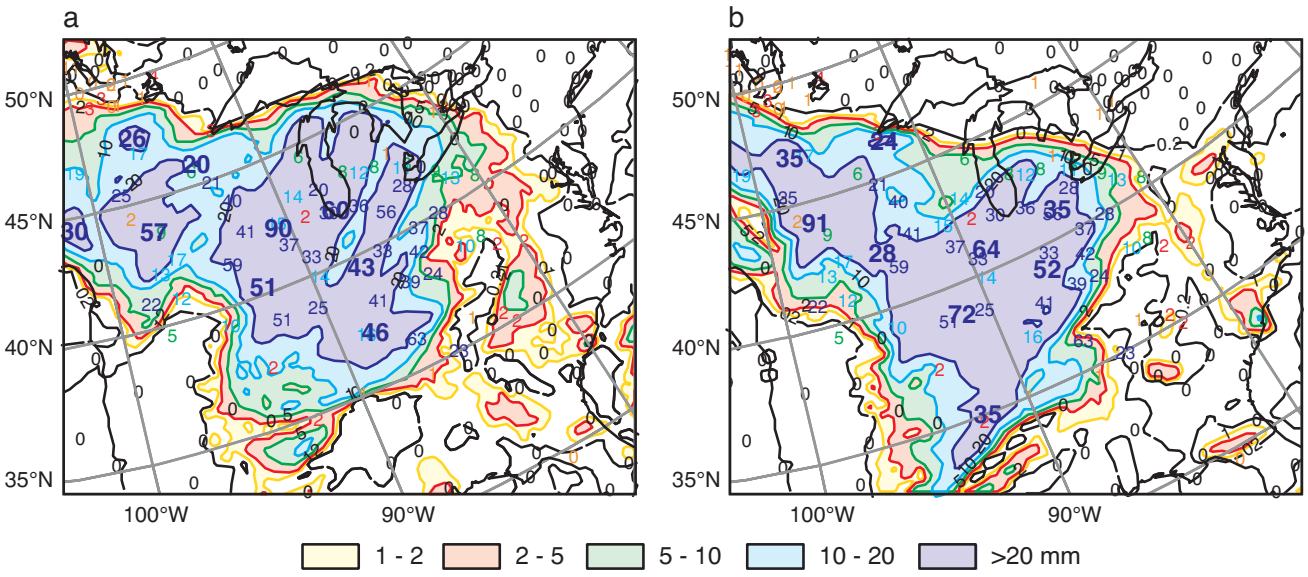

Figure 11 The observed accumulated 24-hour surface precipitation (mm) over the central and eastern USA between 12 UTC 4 May and 12 UTC 5 May (thin coloured numbers), and the 25r4 forecast values (colour shaded areas) for (a) the 60-hour forecast starting at 12 UTC 2 May, and (b) the 36-hour forecast starting at 12 UTC 3 May. The bold blue numbers denote maximum local forecast values.

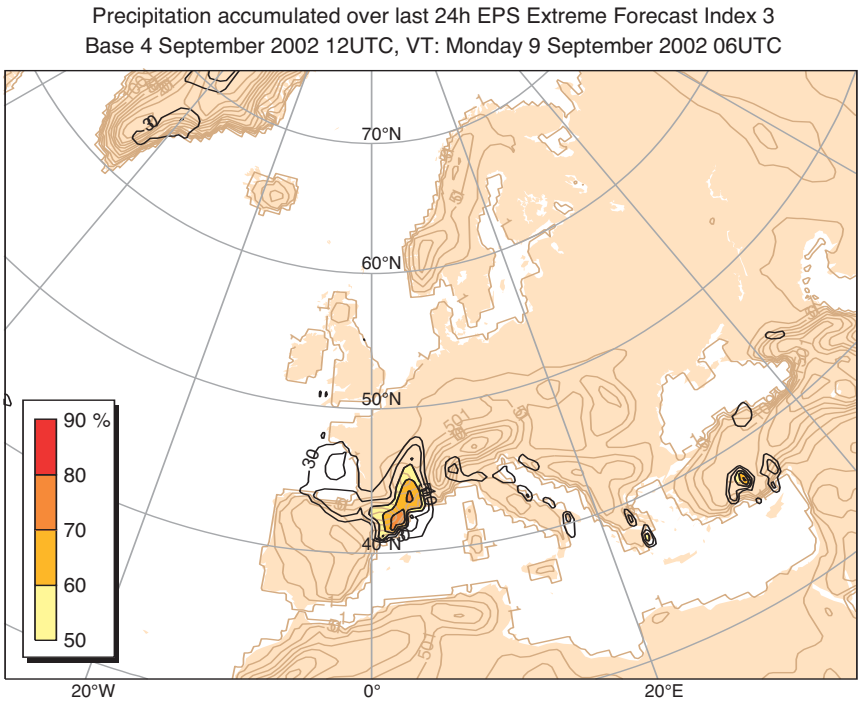

Figure 12 The Extreme Forecast Index map from the ECMWF EPS run starting at 12 UTC 4 September 2002, valid for the 24-hour rainfall for the period ending at 06 UTC 9 September. The index peaks at 100% when all the forecasts exceed values encountered in the EPS runs archived over the recent years.

Finally, the verification of the forecast 24-hour accumulated surface precipitation against surface observations for the period 12 UTC 4 May to 12 UTC 5 May is illustrated in Figure 11. The forecast starting on 3 May (Figure 11(b)) provided a quite realistic picture as it produced a large area south of the Great Lakes with precipitation amounts between 30 and 70mm. The precipitation forecast from 2 May was spatially less accurate, but was still very useful as most of the values are within the range of the observed rainfall amounts.

Forecasting products for severe convection events

Forecasting severe weather events, such as the ones described, three to five days in advance cannot be achieved in any categorical sense. The Ensemble Prediction System (EPS), however, may provide an estimate of the probability that such unlikely, but highly damaging, events will occur. One of the products specifically designed to detect whether the EPS distribution of outcomes deviates significantly from the usual model climatology is the Extreme Forecast index (EFI) (*Lalaurette and van der Grijn* 2002). Figure 12 shows that a signal was indeed detected in the area five days in advance although, at this early stage, the forecast was identifying both the south-eastern part of the Pyrenean range and the Cevennes region (where the intense rainfall actually occurred).

At shorter forecast ranges (two to three days in advance), the deterministic forecast is able to predict reasonably well both the locality and the intensity of these organized severe-convection events (in terms of rainfall, mean low-level wind speed, CAPE, etc.). This has been illustrated in the two events of intense synoptically forced convection over land in Europe and the USA discussed in this article.

Synoptic features, such as mid-level dry layers and vertical wind shear, significantly determine the nature of the convection in terms of surface wind gusts, precipitation efficiency and lifetime of convective systems. However, the forecast model does not provide any diagnostics for wind gusts related to convective draughts, and the forecaster has to estimate these values empirically (a 'wind-gust' parameter is provided to the user community but it is currently based on the 'turbulent' fluctuations of the mean wind). Furthermore, the model can only provide a grid-average (time-average) precipitation rate, so that convective events that are strongly localized in space and time cannot be expected to be reproduced realistically. Finally, further improvements of the deterministic forecasts are expected by ongoing research on the humidity analysis and the assimilation of satellite-derived rain rates.

All products presented here are, or soon will be, available to Member States in the MARS archive and the real-time dissemination.

Further reading

Articles on recent floods

Bechtold, **P.** & **E. Bazile**, 2001: The 12-13 November 1999 flash flood in Southern France. *Atmospheric Research*, **56**, 171-189.

Sénési, **S.**, **P. Bougeault**, **J.-L. Cheze**, **P. Cosentino** & **R-M. Thepenier**, 1996: The Vaison-la-Romaine flash flood: mesoscale analysis and predictability issues. *Weather and Forecasting*, **11**, 417-442.

Articles on convection and severe-weather forecasting

Gregory, **D.**, **J-J. Morcrette**, **C. Jakob**, **A.M. Beljaars** & **T. Stockdale**, 2000: Revision of convection, radiation and cloud schemes in the ECMWF model. *Q.J. Royal Meteorological Society*, **126**, 1685-1710.

Lalaurette, **F.** & **G. van der Grijn**, 2002: Ensemble Forecasts: can they provide useful early warnings? *ECMWF Newsletter 96*, 10-18.

Tiedtke, **M.**, 1989: A comprehensive mass flux scheme for cumulus parametrization in large-scale models. *Monthly Weather Review*, **117**, 1779-1800.

Peter Bechtold, François Lalaurette, Anna Ghelli and Martin Miller

The ECMWF seasonal forecasting system

During 2002, a substantial upgrade was made to the seasonal forecasting system. Changes include the use of a more recent version of the atmospheric model, increased resolution in both the atmospheric and the oceanic models, changes to the parameterisation of the ocean model, a new way of ensemble generation and changes to the way in which the forecast anomalies are calculated and validated. The ocean analysis system has also undergone substantial changes and new products both from the analysis and the forecast system are displayed on the web. A comprehensive User's Guide is available on the web (http://www.ecmwf.int/products/forecasts/seasonal/documentation/), as well as results of an extensive comparison between the current seasonal prediction system and its predecessor.

Description of the ECMWF seasonal forecast models

The original seasonal forecasting system (System 1)

The first seasonal forecasting system at ECMWF was introduced in 1997. A brief summary of this system (known as System 1 or S1) is given here, in order to explain better the changes made for the new system. S1 used Cy15r8 of the IFS, which was the latest version available at the time. The resolution used was T63, with 31 vertical levels. Initial conditions for the atmospheric model were obtained from the ECMWF operational analyses used in the 10-day forecast; these include soil moisture and snow cover as well as upper-air fields. The ocean model was a version of HOPE (the Hamburg Ocean Primitive Equation model), global in extent but with varying resolution. The meridional resolution near the equator was 0.5°, and the mid-latitude resolution was 2°×2°. The ocean initial conditions were obtained from a basic ocean analysis system in which all available in-situ temperature data were assimilated. The ocean analysis was run 11 days behind real time to allow for sea surface temperature (SST) and sub-surface data acquisition.

One coupled forecast was run each day, and ensembles were created by pooling forecasts made over a period of a month. Typically this was done by taking forecasts from the 16th of one month to the 15th of the next, and assigning the ensemble a nominal start date of the 1st of the month. Ensemble forecasts were made in this way from the start of 1997 until S1 was switched off in March 2003. Because of the way the ensemble was built up, a '1 January' forecast was not available until 26 January (11 days lag on the ocean analysis, plus 15 days lag from the ensemble method).

As with all coupled models, the model was not perfect. One symptom of this is climate drift; the model climatology does not match that of nature. To allow for this, the model forecasts need to be referenced to the model climatology. For S1 this was obtained by running an 11-member ensemble for every month of the years 1991–1996. These integrations were all started on the 1st of the month, unlike the real-time forecasts made from 1997 onwards. The data output from S1 was less than ideal; certain fields with important diurnal cycles (such as 2m temperature) were stored as instantaneous fields at 00 UTC only, and the original system did not have a properly designed data archive in MARS.

In summary System 1 was a prototype system and subject to different ensemble generation strategies at different periods in its development. The data archive from S1 was originally scattered across different research and operational archives and, although the archive has since been consolidated, the varying structure of the ensemble and the limited data output make the forecasts from S1 quite difficult to use.

The current operational seasonal forecasting system (System 2)

The current seasonal forecasting system, System 2 (S2), was introduced into operational use at the beginning of 2002. It differs from S1 in a number of ways. The atmospheric component is Cy23r4 of the IFS with a horizontal resolution of T_L95 and 40 levels in the vertical. This is the same cycle of the IFS as was used in the ERA-40 reanalysis. The ocean-model resolution was increased to 0.3° meridionally near the equator and to 1°×1° at higher latitudes; the vertical resolution of the ocean increased from 20 to 29 levels. Changes were also made to the ocean model physics, mainly the parameterisation of vertical mixing.

Substantial changes were made to the ocean assimilation system. The ocean initial conditions are provided not from a single ocean analysis but from a five-member ensemble of ocean analyses. The analyses differ in that a measure of uncertainty in the surface winds used to force the ocean is taken into account. In the absence of ocean data assimilation the uncertainty in ocean state is relatively large, but in the presence of ocean data assimilation it is much smaller. When ocean analyses are displayed on the web, the ensemble-mean is used. There are other differences from the analysis system used in S1. Although only temperature is analysed, salinity is adjusted in such a way as to preserve the temperature-salinity (T-S) relationship, and the velocity is corrected following a density update. Ocean analyses are now carried out only down to 400 m and the background-error covariance scales have been reduced slightly.

The ensemble ocean analysis is part of the new method of ensemble generation in S2. Each ensemble forecast consists of 40 members, all with initial conditions on the 1st of the month. Our aim is to explicitly construct this ensemble to represent the most important uncertainties in the initial conditions as best we can. There is certainly scope for improving the methods by which we do this, but we expect the new strategy of explicit ensemble construction to be a feature of all our future seasonal forecast systems. Despite using what we consider to be the best SST analysis available, the errors in the weekly mean values are estimated to be of the order of 0.2 – 0.3 K. To represent this uncertainty, 40 different SST perturbations are created and added to the five ocean analyses, to create a 40-member set of ocean initial conditions from which the forecasts are launched. In addition, stochastic physics is used to perturb the coupled integrations through-

out the forecast period. This gives a significant de-correlation of the atmospheric flow in the tropics in the first few days of the forecast, compensating for the fact that we do not include perturbations to the atmospheric initial conditions. The 40-member ensemble can be run once the ocean analyses are available, generally on the 11th of each month. Because a large amount of computation is involved, and to ensure reliable delivery, the operational release date for the forecast is set at the 15th of the month; this is still a big improvement in timeliness over our first system.

The calibration integrations for S2 span the years 1987 - 2001 when an ensemble of five members is created, one from each of the ocean analyses. This 15-year climate gives a more stable basis for computing anomalies than the 6-year climate available in S1. For a further description of S1 and S2, including an assessment of their different characteristics see *Anderson et al.* (2003).

Accessing data and products

A selection of graphical products from the seasonal forecast system is displayed on the ECMWF web pages. All plots can be downloaded as postscript or pdf files, as well as being viewed on screen. As before, spatial maps of 2m temperature, precipitation and mean-sea-level pressure are shown, but now in the form of probabilities for tercile and 15 percentile categories, as well as the ensemble-mean anomaly and the probability of exceeding the climate median. The Niño SST indices include the Niño 3.4 and Niño 4 regions as well as Niño 3, and the ocean-analysis plots include several meridional sections, as well as zonal and horizontal maps.

One new type of forecast product is the 'Climagram', which shows both the forecast probability distribution function (pdf) and the climatological pdf. This enables the user to assess at a glance the importance of any predicted shifts in the pdf of the variable concerned. These climagrams were in part inspired by the work done at MétéoSwiss, and are created for precipitation, 2m temperature, and SST anomalies averaged over several areas, and three large-scale atmospheric indices: the Southern Oscillation Index (SOI), the North Atlantic Oscillation (NAO), and the Pacific North American pattern (PNA). As an example, Figure 1 shows the climagram for the SOI predictions started in December 2002. In the first month, the forecast median (blue line inside the box) is well below the climatological median (red line). During the forecast the distance between the two medians decreases rapidly and, by April, the forecast distribution has values similar to the climatological one. This change of the SOI from negative to near normal is consistent with the rapid decay of El Niño conditions.

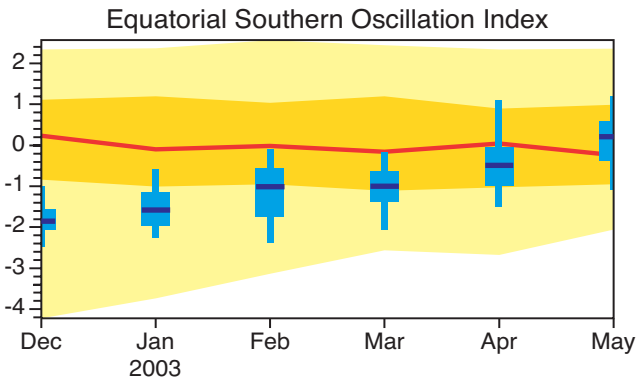

Figure 1 A climagram, showing Southern Oscillation Index predictions from December 2002. Predicted monthly-mean values are represented in blue and model climatological values are in yellow. The climate extremes (95% and 5%) are described by the limit of the light yellow shading, the dark yellow band is limited by the 75% and 25% climate values and the climate median is the thick red line. The forecast ensemble distribution is represented by blue boxes with upper and lower values corresponding to 75% and 25%, the forecast median is represented by the blue line and forecast extremes (95% and 5%) are represented by the whiskers.

The operational system, S2, has a better data archive than S1, and we now encourage users of the seasonal forecast system to consider accessing and using the data directly, in addition to the graphical products on the web. S2 archives a large number of different model fields, although only a small subset of these is presently listed in the 'ECMWF catalogue' for commercial use.

Each ensemble member archives data at 6/12/24 hour intervals, depending on the field concerned. A full list of the output fields can be found in section 3 of the on-line Seasonal Forecast User Guide. The comprehensive data archive allows the development of a full range of sophisticated products, and in particular the synoptic variability of each ensemble member is well resolved. The upper air and surface fields should be sufficient for statistical downscaling techniques, including those that require the synoptic evolution of the system. The archive does not include the full model level data that would be required to drive regional dynamical models, since to store the full global fields for all ensemble members would be excessive.

When developing seasonal forecast products, the model forecast values must always be interpreted in the context of the model output in previous years. Five-member 'back-integration' ensemble forecasts for the years 1987–2001 are available in the archive, with the same output as the real-time forecasts. Both real-time forecasts and back integrations are retrieved from MARS in the same way. For example, the following would retrieve the first few days of daily maximum 2 m temperatures, first from the forecast and then from the back integrations:

```
retrieve,
  stream=seas, system=2, method=1, number=0/to/39,
  class=od, expver=1, date=20030401, time=0,
  type=fc, levtype=sfc, param=201, step=24/48/72/96,
  target=2m_tmax_forecast
retrieve,
  number=0/to/4,
  date=19870401/19880401/19890401/19900401/19910401/19920401/
       19930401/19940401/19950401/19960401/19970401/19980401/
       19990401/20000401/20010401,
  target=2m_tmax_climate
```

In this retrieval, note the use of 'stream=seas' to indicate that it is the seasonal forecast we want, 'system=2' to indicate that it is the system 2 data, and 'method=1' to indicate that it is the main set of forecasts required. (There are some method=0 forecasts in the archive, which do not use in-situ data to create the ocean initial conditions and are not recommended for general use; in the future, there may be method=2/3/4 etc as part of a multiple forecast system). Note also that all seasonal forecasts start at 00 UTC.

The full temporal-resolution data is powerful, but the large and complex data volumes are not always easy to work with and, in the majority of cases, something simpler is wanted. To help with this, the monthly means of all forecast quantities are also calculated and stored in MARS, in stream=sfmm (seasonal-forecast monthly mean). Several 'types' are available, including fcmean (forecast mean), fcmax (the maximum value of the field occurring during the month) and fcmin. The mean values are calculated from the available high-frequency data. For example, the monthly mean 2 m temperature is the mean of all of the six-hourly instantaneous values within the month, thus including both night-time and daytime values. For accumulated fields, such as solar radiation or precipitation, the monthly means contain the mean rate of accumulation during the month. For fluxes, the values are thus in convenient units (W/m^2), but precipitation values need scaling (from m/s to, for example, mm/day). The month(s) to be retrieved are specified in terms of time into the forecast with 'fcmonth'. A typical retrieval of six months' data will look like:

```
retrieve,
  stream=sfmm, system=2, method=1, number=0/to/39,
  class=od, expver=1, date=20030401, time=0,
  type=fcmean, levtype=sfc, param=201, fcmonth=1/2/3/4/5/6,
  target=2m_tmax_monthly
retrieve,
  number=0/to/4,
  date=19870401/19880401/19890401/19900401/19910401/19920401/
       19930401/19940401/19950401/19960401/19970401/19980401/
       19990401/20000401/20010401,
  target=2m_tmax_monthly_clim
```

Note that, in this retrieval, we again get the data from the 'back-integration' forecasts, so that we can properly interpret the real-time model output. Finally, for a selected number of fields (including all those in the commercial catalogue), pre-calculated monthly-mean anomalies are available in stream=smma, and pre-calculated ensemble means (type=em) are available for both monthly anomalies and monthly full fields. Ocean data from the forecasts are accessed as 'stream=seas, levtype=depth' and wave-model data are in stream=wasf and stream=swmm for daily and monthly mean values respectively.

For anyone starting to work directly with the model data, a good test is to try to reproduce some of the plots from the ECMWF web pages. We use a 75-member climate of forecasts from the years 1987–2001, and the 40-member real-time ensemble. The significance masking on the ensemble-mean plot may not be easy to reproduce, but the Prob>median plot should be manageable. Seasonal forecasts are available at 12 UTC on the 15th of the month, and this applies both to the plots on the web and the retrieval of data from MARS.

Ocean analysis data are also archived in MARS, again in 'stream=seas'. The ocean analyses are 'type=an', and are produced daily. As well as the ocean model level data, a subset of other ocean diagnostics is available, such as different zonal and meridional sections, time-space sections, and accumulated fields. For further details see http://www.ecmwf.int/products/forecasts/seasonal/documentation/ch3_2.html

Assessment of performance

It is natural to compare the performance of the new operational system, S2, with that of its predecessor S1. Here, we discuss the skill in predicting the SST, since this is the foundation of any ability to predict atmospheric anomalies. We then briefly describe some of the performance and skill statistics that are available on the web for both the old and new systems. Those interested in a more thorough discussion of the differences in performance between S1 and S2, including the performance in the 1997/98 El Niño, are invited to download Tech Memo 404 from the ECMWF web site (http://www.ecmwf.int/publications/library/do/references/list/) and to read the article by *van Oldenbergh et al.* on page 26 in this issue of the Newsletter.

SST forecast skill

Many changes have been introduced to the atmospheric model since Cycle 15r8, and changes have been made to the ocean model and assimilation system also. Although the changes to the atmospheric model have been beneficial in terms of medium-range weather forecasts, it is not automatic that the combined effect of the atmospheric and oceanic changes will increase seasonal forecast skill. Figure 2 shows the correlation of predicted SSTs with observations for forecasts started between 1991 and 2001 for both S1 and S2, and shows the general broad similarity of skill between the two systems. More precise comparisons are possible by looking at the error statistics of ensemble-mean SST forecasts in specific regions. Figure 3 shows results for the Niño-3 and Niño-4 regions, defined in Figure 4. Figure 3 shows that S2 is better than S1 in Niño-3 but that it is worse than S1 in Niño-4, consistent with the correlation skill shown in Figure 2.

The biases in surface temperatures are reduced in S2. For example, shown in Figure 5 is the mean error in surface temperature, six months into a coupled model forecast for (a) S1 and (b) S2. The biases in surface temperature are large, especially over land. Errors over the ocean may look smaller, but are still significant compared with the size of interannual variability in SST. Figure 5(b) shows that the bias is considerably reduced in the new coupled model, particularly over the tropical oceans.

Although the temperature biases in S2 are reduced relative to S1, and the forecasts of Niño 3 SST are, on average, improved, not all aspects of the new system are as we would like them. One problem is that the amplitude of SST variability is too small in S2 – the model is not able to develop or sustain SST anomalies as large as those seen in the 1997 El Niño. Part of the reason for this is that the winds in the atmospheric model do not respond to changing SST anomalies as vigorously as observations suggest they should. The

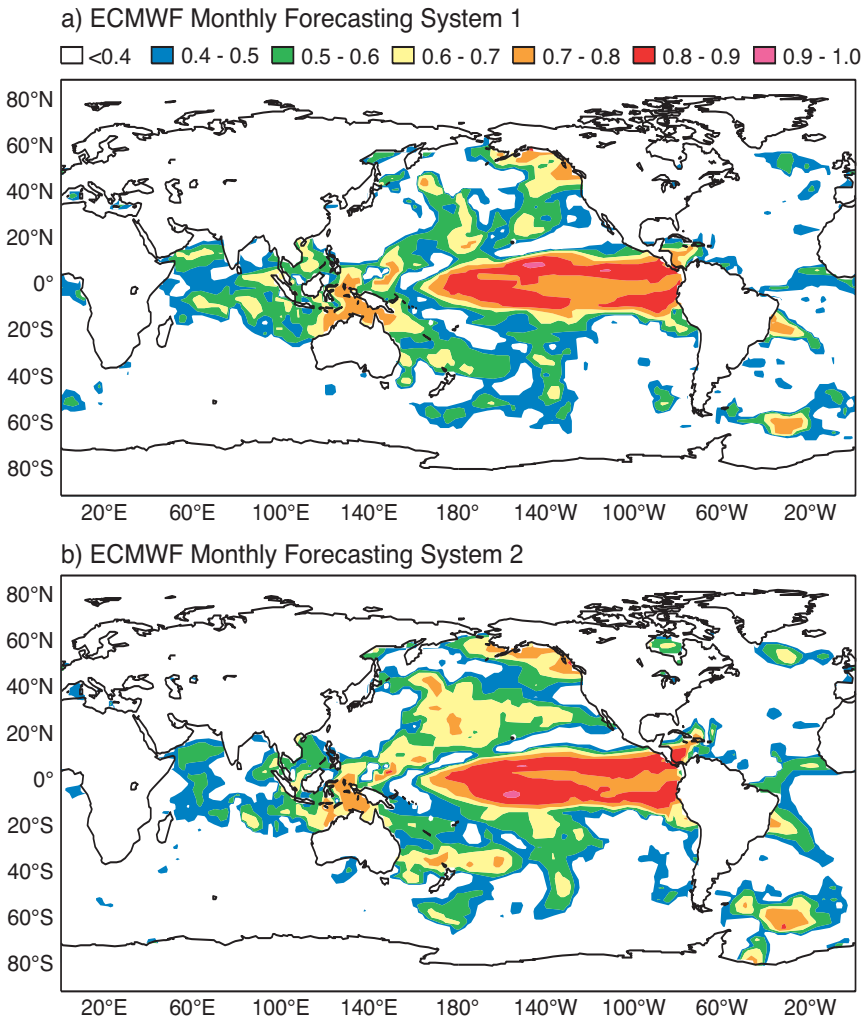

Figure 2 Spatial map of the temporal anomaly correlation between forecasts and observations of SST anomaly, for the forecasts for months 3-5 and for the years 1991–2001 for (a) S1 and (b) S2. The two forecast systems have broadly comparable skill in pretty much the same regions. There is a hint that S2 is better in the central east-equatorial Pacific but worse in the west.

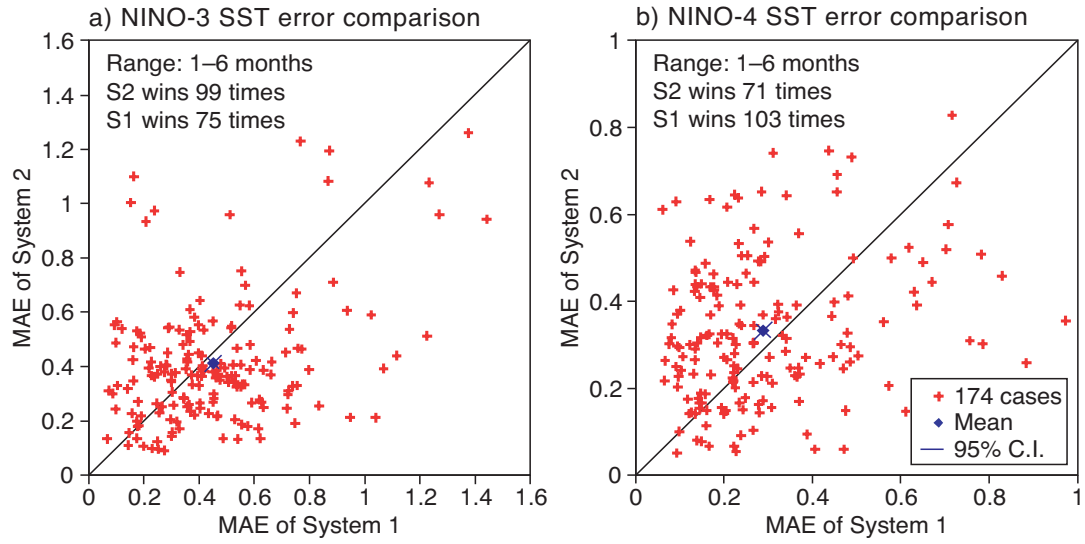

Figure 3 Scatter plot of the mean absolute error for forecasts covering the period 1987–2001 for S2 versus S1: (a) Niño-3, and (b) Niño-4. The blue diamond marks the centroid, with the arms of the cross indicating the 95% confidence interval for the position of the centroid. In Niño-3, S2 is more skilful than S1 but in Niño-4 the opposite is true.

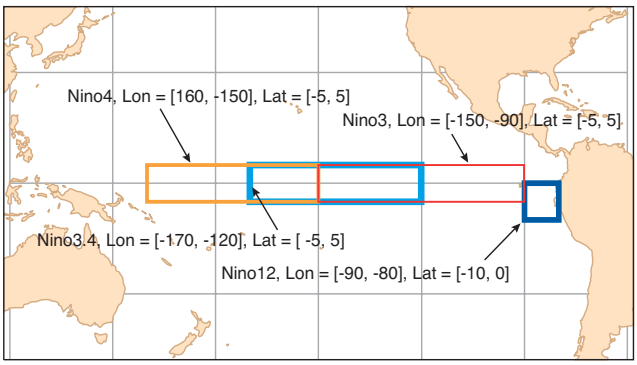

Figure 4 Plot of Niño-3, Niño-3.4 and Niño-4 regions in the equatorial Pacific.

cause of the reduced wind variability is not entirely understood, and may not be helped by the drift in the coupled model, but it is substantially present even in uncoupled integrations of the atmospheric model. Part of the reason that S1 gave well-balanced forecasts in the Niño-3 region was due to the way that the errors in the atmosphere and ocean models almost compensated each other. This is the archetypal reason why improving coupled models is hard; real improvements in one part of the system can so easily lead to problems with some aspects of performance of the system as a whole.

SST forecast spread

We frequently find that the observed SST anomaly in the Niño regions lies outside the ensemble. Our strategy with the seasonal forecast system is to represent the uncertainty in the initial conditions, and calculate the amount of uncertainty this produces in the forecast. If the observed SST anomaly is often outside the predicted range or, equivalently, the forecast error is generally bigger than the forecast spread, then our forecast errors are larger than they need to be, and/or we are overestimating the predictability of the system. This is the case with both S1 and S2.

As mentioned earlier, the forecast ensemble is constructed to represent uncertainty in the ocean sub-surface conditions and in SST, and stochastic physics is also active. We have studied the impact these different perturbations have on the apparent predictability of the system in a series of experiments. Figure 6 shows the growth of error over the first month, and over six months, resulting from the wind perturbations, the SST perturbations, stochastic physics, all three together, and the lagged-average approach (mimicking the ensemble method used in S1). Wind perturbations and stochastic physics lead to similar growth rates in Niño-3. They start from small spread in SST and it takes about three months to reach a spread comparable to that of the SST perturbations or lagged-average approach. A further experiment using wind and temperature perturbations and stochastic physics, but in the absence of ocean data assimilation, is also shown. Comparison of the light blue curve with this (mauve) curve gives a measure of the degree to which data assimilation has constrained the spread generated by the wind perturbations in the ocean analyses. The wind and SST perturbations that we apply are thought to be either a fair or an overestimate of the true

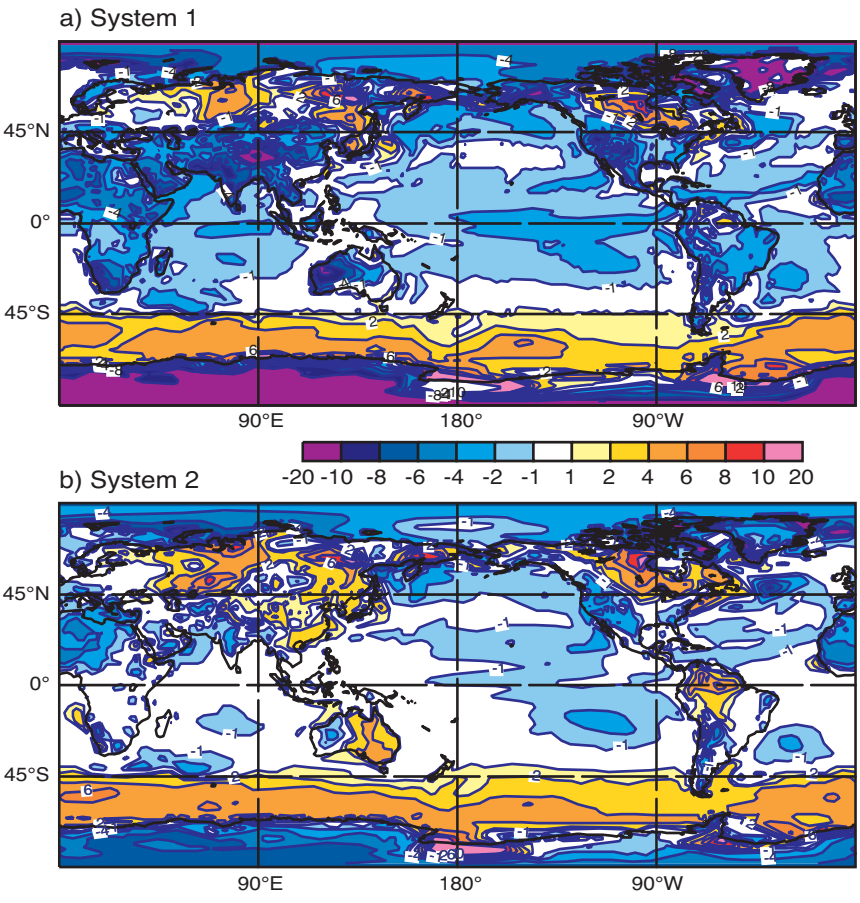

Figure 5 The bias in surface temperature after six months for (a) S1 and (b) S2. The reference climatology is ERA-40.

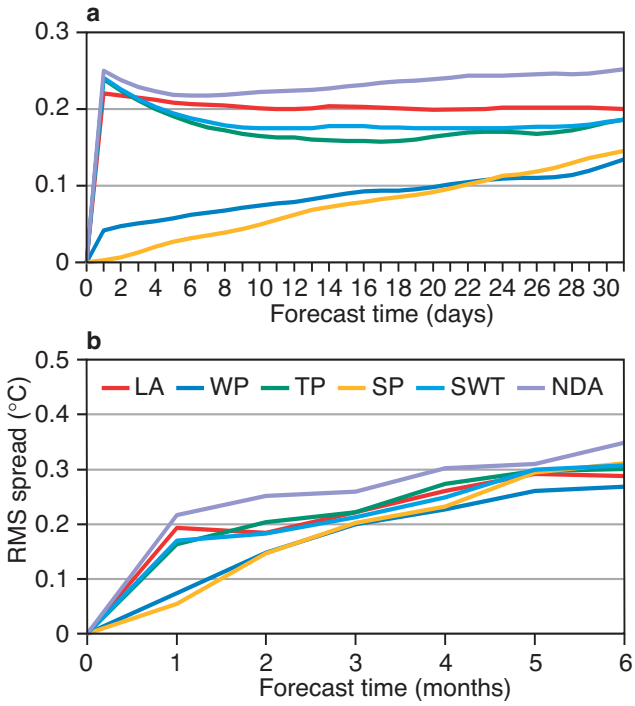

Figure 6 Plot of the error growth and of the ensemble spread in Niño-3 as a function of lead-time for various methods of generating ensembles. LA corresponds to lagged average, WP to wind perturbations, TP to temperature perturbations, SP to stochastic physics, SWT to stochastic physics, wind perturbations and temperature perturbations, and NDA to the equivalent of SWT but without ocean data assimilation. Wind perturbations are applied during the ocean-analysis procedure, temperature perturbations are applied to the surface temperature at the initial time only and stochastic physics is active throughout the coupled model integration.

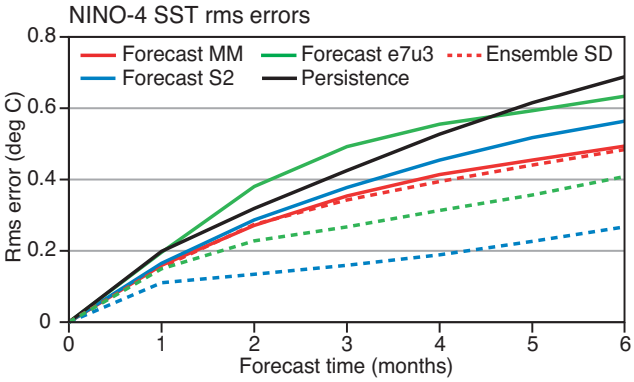

Figure 7 Plot of the error growth in Niño-4 for S2 (solid blue curve) and of the growth of the ensemble spread (dashed blue). Green, as for blue but for the Met Office model, and red for the two-models combined. The spread of the Met Office forecasts is larger than for ECMWF as is the rms error, but the error is reduced in the two-model case and the spread matches the error.

uncertainties. The actual growth rate of the perturbations is partially model dependent, and not all types of initial-condition errors are represented in our ensemble, but it is clear that a substantial part of our forecast error is not due to initial-condition error, but to errors in the coupled model itself.

The belief that model error is a significant source of forecast error clearly has implications for our future development strategy. But it also leaves us with an immediate dilemma: what can we do to make our ensemble forecast give a better representation of the range of possible outcomes? One possible approach is to inflate the ensemble spread based on past errors, but if the past errors are relatively large, this will result in a very wide spread. Alternatively, we can try to construct a multi-model ensemble, that is a forecast made from an ensemble of different models. The concept is illustrated by Figure 7, which shows the uncalibrated root-mean-square (rms) errors and spread from two different forecast models (S2 in blue, UK in green). The UK model has both a larger spread and larger errors than S2, but a comparable level of inconsistency between spread and error. The red curves show the spread and the error for the multi-model ensemble, i.e. an ensemble consisting of both sets of forecasts. The rms errors of the ensemble-mean forecast are smaller than for either individual model, and the spread in the ensemble much more closely matches the forecast error. It is not shown here, but the anomaly correlation is also generally increased. This example uses only two models, but a significantly larger number of models is desirable. The multi-model approach is useful for a wide range of atmospheric variables, not just SST. Further work on ensemble generation and real-time multi-model product development is in progress. A future Newsletter article on the DEMETER project will address the multi-model approach to seasonal forecasting in greater detail, using a series of hindcasts covering the last 43 years.

The 2002 El Niño

There was a moderate El Niño event in 2002 peaking around December 2002. The forecasts for Niño-3.4 have generally been good for this El Niño. Figure 8 shows Niño-3.4 predictions throughout the year with subsequent verification (heavy blue line). An interesting point was reached in December 2002, when there was considerable speculation that El Niño would intensify in response to a pattern of wind variability that had propagated to the Pacific from the Indian Ocean. In contrast to such speculation, the ECMWF forecasts showed no intensification of El Niño, but rather a relatively rapid decline from November / December, which has subsequently verified well. Although the Niño-3.4 forecasts were generally very good, some other regions showed errors: Niño-4 forecasts underestimated the persistence of warm conditions in the early months of 2003, for example. This error was perhaps consistent with our earlier finding that S2 does not perform particularly well in this region. At the time of writing (June 2003), there is again much speculation about the likelihood of La Niña conditions (cold SST) developing in the latter half of 2003. The ECMWF forecasts have a relatively large spread, and suggest that, while La Niña conditions are possible, a more likely scenario is for SSTs not to be too far from normal.

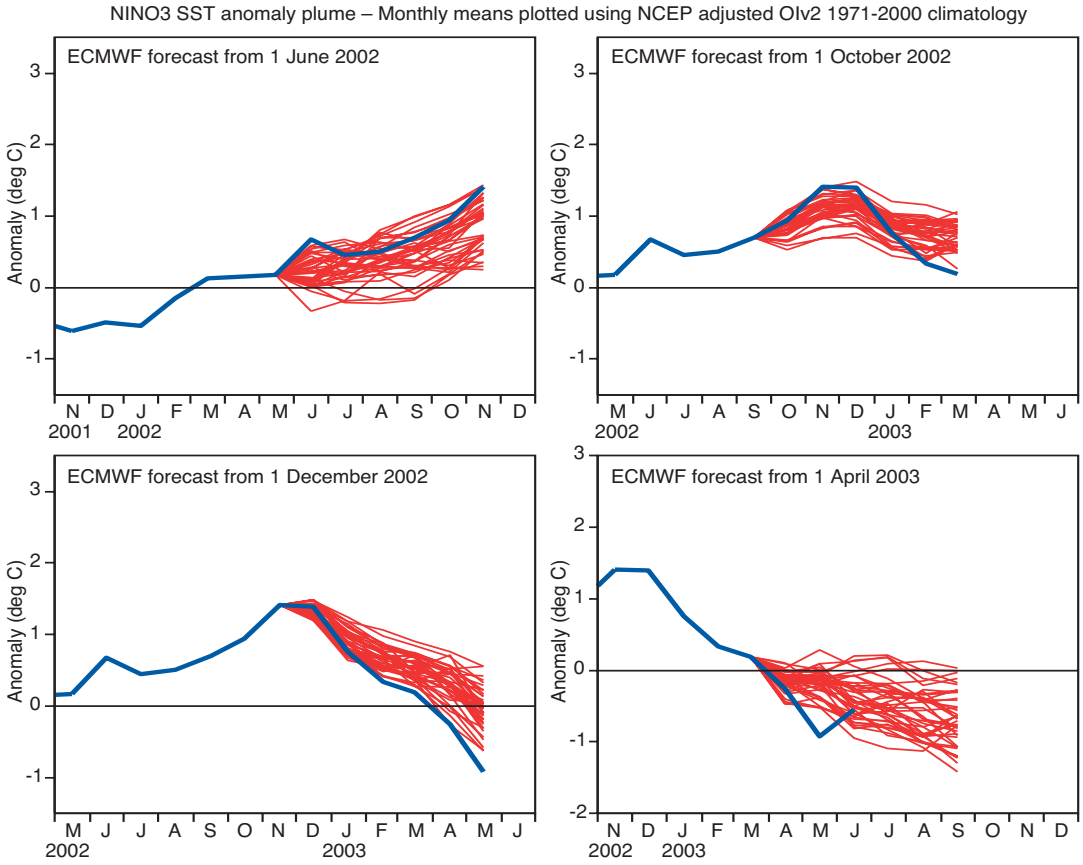

Figure 8 Plot of forecasts of Niño-3.4 at four start dates June, October, December 2002, and April 2003. The red lines represent the 40 ensemble members. The heavy blue line represents subsequent verification. The forecasts from November (not shown) and December 2002 were especially good, but in general the observations often lie outside the predicted range.

Verification

For a correct interpretation of seasonal predictions the user needs to complement the forecast products with knowledge of the forecast skill. The site at http://www.ecmwf.int/products/forecasts/d/charts/seasonal/verification/ provides a comprehensive documentation of skill levels, using methods that have been agreed at the international (WMO) level for the evaluation of long-range forecast systems. Estimates of model bias for a wide range of variables, including zonal averages, time series of a set of indices of SST and large-scale patterns of variability, such as the SOI, the PNA and the NAO, are available. A suite of verification scores for deterministic (e.g. spatial anomaly correlation and mean-square skill-score error (MSSS)) and probabilistic forecasts can be viewed. This site, which contains verification for both the operational system, S2, and the 'old' system, S1, has benefited from developments in the framework of the DEMETER project.

The robustness of verification statistics is always a function of the sample size. For the operational seasonal forecast system, the sample size of 15 years is considered barely sufficient. Verification is performed in cross-validation mode using the whole set of forecast data available: hindcasts and real-time forecasts with no distinction. Since the seasonal forecast skill depends very strongly on the season, forecasts started in February, May, August and November are evaluated separately. Results are shown as 90-day means with one- and three-month forecast leads. Global Precipitation Climatology Project (GPCP) data are used to verify precipitation, while the other atmospheric parameters are verified against ERA-40. For the period when the reanalysis is not yet available, the operational analysis is used. The verification period is 1987 to 2002 for S2, and the more limited period 1991 to 2002 for S1. Every year, the site will be updated by adding another year to the verification period. The maximum number of forecasts available for the entire verification period is used. For example, for S2 only five members are considered, since in the period 1987–2001, only five members are available. However, for the forecasts started in November and May ensembles of 40 members are available; so for these particular forecasts all the 40 members are included in the verification. The ensemble for S1 consists of 11 members.

Although we can take advantage of the experience in the medium-range forecast verification, evaluating seasonal forecast skill involves dealing with a generally small signal-to-noise ratio and a limited sample of cases. Significance testing methods are, therefore, particularly relevant and this is something we hope will be increasingly reflected in the verification statistics provided to our users.

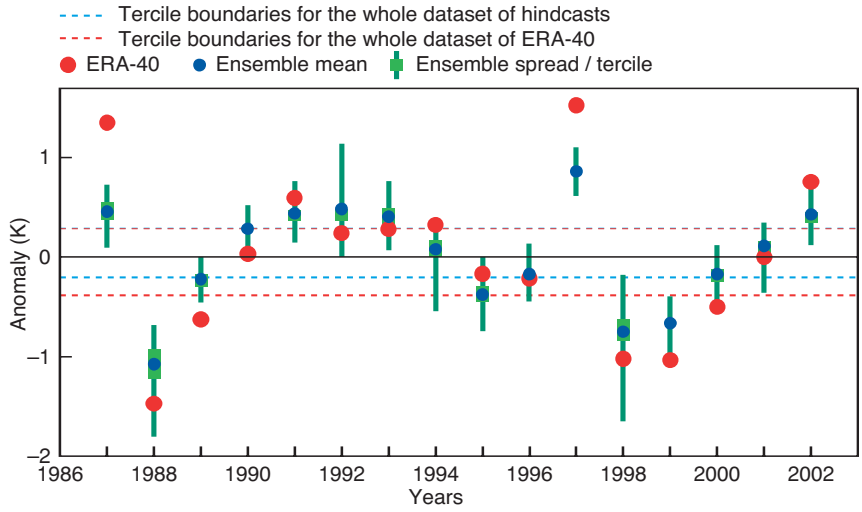

Figure 9 Verification (red dots) of Niño-3.4 SST forecasts from the operational system. The ensemble mean is given by the blue dots, and a measure of the spread by the green bars.

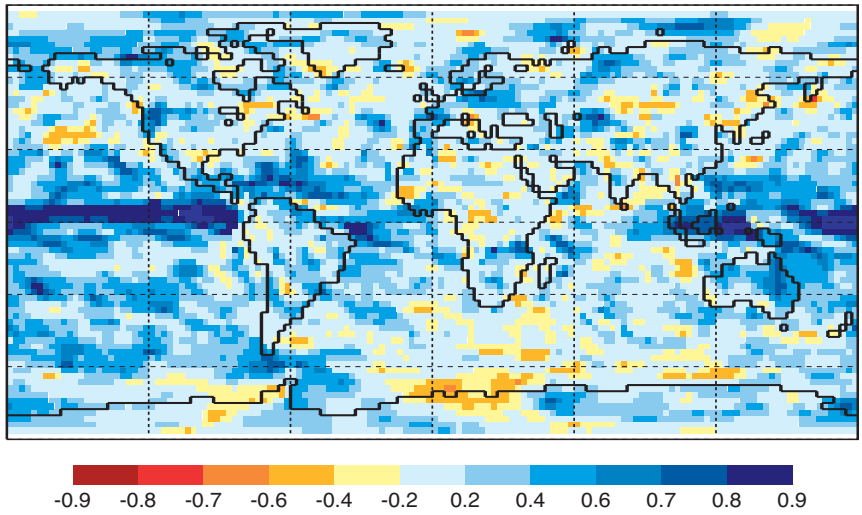

Figure 10 Map of temporal anomaly correlation of precipitation for June–July–August forecasts starting in May for the period 1987-2001.

Bias maps

Spatial distribution of the mean errors (biases) are provided at http://www.ecmwf.int/products/forecasts/d/charts/ seasonal/verification/bias/ although it should be understood that such biases are removed from the forecast products as part of the post-processing. Nonetheless, information on model drift is useful for diagnostic purposes. Zonal-mean biases are also computed for the whole latitudinal band and for the Atlantic and Pacific regions.

Forecast indices

Time-series anomalies of several indices describing the oceanic and atmospheric conditions averaged over three-month periods are available. The Niño-3.4 verifications for May forecasts are shown in Figure 9, for example.

Single-value forecast scores

The most usual way to summarise the information from an ensemble of forecasts into one value is to use the grand mean of all members. Although such values are often referred to as deterministic forecasts, the grand mean acts to remove random unpredictable errors from the forecast. As a consequence, ensemble-mean charts are unrealistic if compared with analyses (many small-scale features do not show up), but they are usually the best single-value estimates if evaluated using rms error measures. For such forecasts, verification of anomaly correlation and MSSSs based on the all years available are provided, both as global maps and averaged over pre-defined areas. An example of an anomaly-correlation map is shown in Figure 10 for precipitation for forecasts started in May for the period 1987–2001.

Probabilistic scores

The full content of the information provided by the seasonal ensemble forecasts is only accessible in multi-valued probabilistic mode. Basic methods for verifying probabilistic forecasts have been in use for several years at ECMWF for medium-range EPS products and the methodology is now being naturally extended to seasonal forecasts. The Relative Operating Characteristics (ROC) curve shows, for a range of different probability thresholds, hit-rates versus false-alarm-rates of forecasts of a particular event in different regions. The event thresholds are defined with respect to terciles from model and verifying climatologies. The blue dotted lines indicate the 95% confidence interval for the hit-rate values. Figure 11 shows the ROC diagrams for 850 hPa temperature summer forecasts for the northern hemisphere as a whole (upper panel) and for Europe (lower panel). This

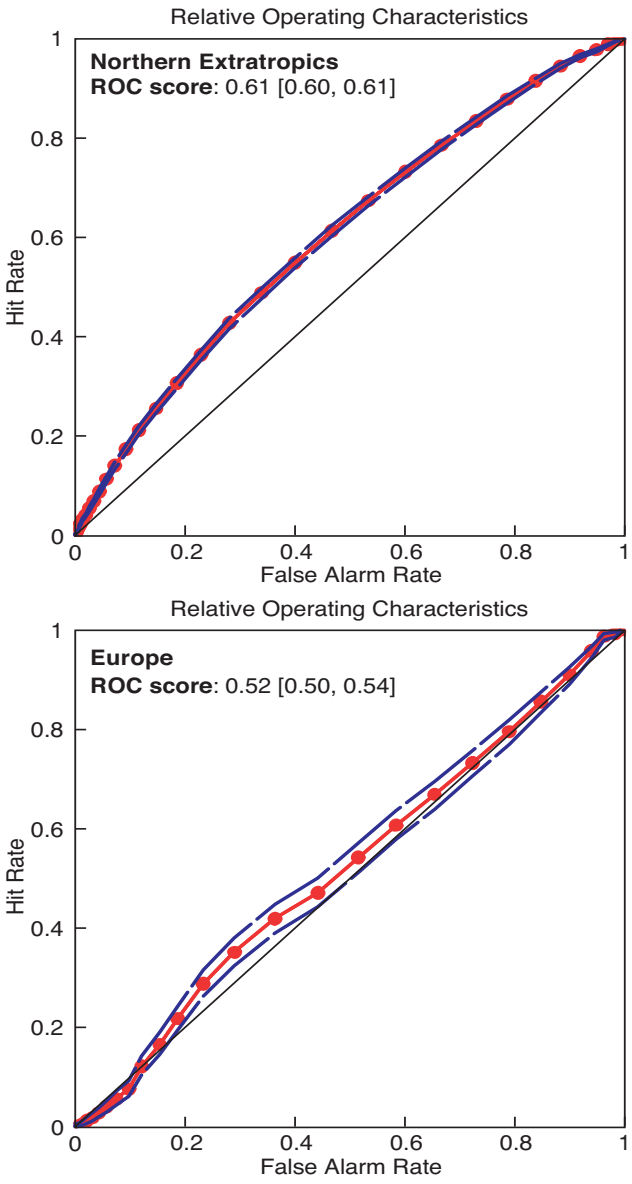

Figure 11 ROC diagrams for 850 hPa temperature anomaly being in the upper tercile. The forecasts are for a lead time two-to-four month forecasts (i.e. June–July–August for forecasts starting in May) for the period 1987–2002. The upper panel is for the northern extratropics and the lower panel is for Europe.

figure exemplifies that, on average, there is skill in predictions several months ahead for the extratropics but that for some regions, such as Europe, forecast skill is limited. It is likely that the skill varies with season and predictand, but it is also likely that the limited sample size makes our skill estimates noisy. Figure 12 is a ROC curve for the prediction of tropical rainfall anomalies for June-July-August. The forecasts start on 1 May for the years 1987–2001. (The verification data are not available for 2002). Figure 12 indicates that there is skill in the forecast of rainfall anomalies in the tropics, even though rainfall is a very chaotic variable. Grid-point values of ROC scores and later ranked probability skill scores are also available on the web as global maps.

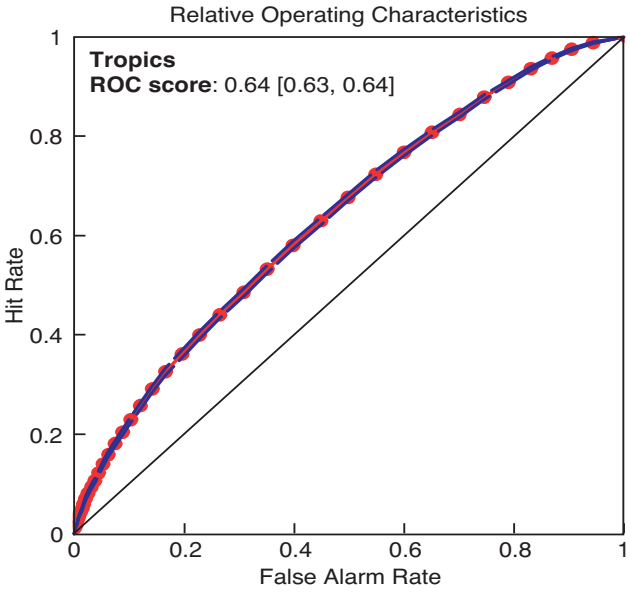

Figure 12 ROC diagrams for the tropical-rainfall anomaly being in the upper tercile for forecast lead of two to four months for forecasts originating in May 1991–2001.

Future developments

The new seasonal forecasting system at ECMWF gives users access to a much wider range of products and data, and much better information on the performance characteristics of the system. Its ability to forecast El Niño type SST variability is well established, although the forecasts are not yet completely reliable. Based on a limited sample of ~15 years, the statistics suggest that there are many areas and parameters for which the atmospheric forecasts also have some skill, but the results are geographically variable and subject to sampling error. Model error is a serious source of forecast error but this can be partly addressed by the use of several models. In the near future we plan to include the Met Office model as part of the seasonal forecasting system, and hopefully to include other models later. There is much work still to be done, but we are confident that we will continue both to improve our model forecasts, and to improve our ability to represent the forecast uncertainties.

Acknowledgements

We acknowledge input from the whole of the Seasonal Forecasting and Demeter teams, and the substantial work by the Met Apps and Met Ops sections in implementing the new seasonal system.

Further reading

Anderson, D., T. Stockdale, M. Balmaseda, L. Ferranti, F. Vitart, P. Doblas-Reyes, R. Hagedorn, T. Jung, A. Vidard, A. Troccoli & T. Palmer, 2003: Comparison of the ECMWF seasonal forecast Systems 1 and 2, including the relative performance for the 1997/8 El Niño. *ECMWF Tech Memo 404* (available on line at http://www.ecmwf.int/publications/library/do/references/list/).

David Anderson, Tim Stockdale, Laura Ferranti & Magdalena Balmaseda

Did the ECMWF seasonal forecast model outperform a statistical model over the last 15 years?

Dynamical vs statistical forecasts

Seasonal forecasts are possible whenever the chaotic weather is perturbed in a predictable way by slowly varying boundary conditions, such as sea surface temperature (SST) or land conditions. The most important of these boundary conditions is the El Niño – Southern Oscillation (ENSO). Although the weather is highly non-linear, perturbations to the average weather can often be taken as being proportional to the forcing, plus unpredictable weather noise. This means that simple, often linear, forecast models can be very useful in seasonal forecasting. In fact statistical models based on linear ENSO teleconnections are used in many locations throughout the world.

In contrast, the ECMWF seasonal forecast model consists of an ensemble of integrations of coupled global circulation models (GCMs) of the ocean and atmosphere (*Anderson et al.* 2003). If the model were perfect, this approach would yield better forecasts, both for ENSO itself and for the teleconnections that give rise to seasonal forecasts, as all physical processes thought to be relevant are included. There has been some debate as to whether today's models are good enough for the advantages of a more complete model to outweigh the errors introduced into the forecast by the model failings. *Landsea and Knaff* (2000), for instance, argued that a simple statistical forecast model predicted the 1997/98 El Niño at least as skilfully as the big dynamical models.

To investigate this issue, we made a systematic comparison of the skill of the ECMWF seasonal forecast models against a set of statistical models, both for ENSO predictions and for the resulting seasonal forecasts. The statistical seasonal forecast model (STAT) consists of persistence and lagged regressions against the first few empirical orthogonal functions (EOFs) of SST, fitted over 1901–1986. The first EOF is the El Niño pattern, the second one the wider decadal ENSO-like pattern. For ENSO forecasts, we also consider damped persistence and the Landsea and Knaff ENSO-CLIPER model that is based on 14 potential predictands.

One problem in seasonal forecasting is the lack of data for a thorough verification. The skill depends very strongly on the season, so that different seasons cannot be combined. This means that during the verification period 1987–2001 only 15 cases of each season are available to compute a skill score. We therefore take the simplest possible measure of skill: the anomaly correlation of the ensemble mean. This means that we assume that biases in the mean state and variance are known and corrected for. The anomaly correlation coefficient (acc) has large uncertainties in samples this small; the (one-sided) 95% confidence level for a true skill of zero goes up to acc = 0.44! When considering large numbers of possible regions and seasons it is, therefore, inevitable that some areas of relatively high correlation would occur by chance even in a system with little real skill.

For this article we restrict ourselves to known ENSO teleconnections in order to reduce the probability of finding high skill scores by chance. By looking only at the anomaly correlation, a deterministic measure of skill, we also ignore the probabilistic aspect of the forecasts. There are other measures that consider patterns rather than the pointwise comparisons implied in an anomaly correlation. A more wide-ranging review of the performance of the ECMWF seasonal forecast system, including probabilistic skill scores and more mid-latitude information, can be found in this issue of the Newsletter by *Anderson et al.* (page 17). Full sets of probabilistic skill plots are available on the ECMWF web pages, at http://www.ecmwf.int/products/forecasts/d/charts/seasonal/verification/.

El Niño - Southern Oscillation forecasts

The hindcasts of the current seasonal forecast system (S2) and the statistical forecast system (STAT) of the Niño3 index (SST anomalies averaged over 5°S – 5°N, 150° – 90°W) over 1987–2001 are shown in Figure 1. The differences between the two are immediately obvious. Although S2 is too strongly damped, it correctly predicted the onset and decay of most El Niño and La Niña events. The exceptions are the failure to predict the 1987 El Niño and the tendency in 2001 to start the 2002 El Niño too early. In contrast, the SST-based statistical model fails to catch the beginning of most events.

The same difference in behaviour can also be seen in the skill as a function of the target season, with an example for lead time +3 months (months 4–6 in ECMWF conventions) shown in Figure 2. The strong drop in prediction skill of the SST-based statistical models for forecasts through the boreal spring is known as the spring barrier. This predictability barrier is much reduced in the dynamical ECMWF model. The use of subsurface information in a full ocean GCM allows predictions with skill only slightly lower in forecasts for the summer than for other seasons. In making forecasts of SST for the boreal winter, however, the statistical models do just as well as the coupled GCM.

Temperature forecasts

We consider the two-metre temperature T2m, and verify against the NCEP/NCAR reanalysis. Over the oceans T2m is highly correlated with SST. The results from forecasts from 1 October start dates for December – February are shown in Figure 3. One sees that SST in the Indian, Pacific and equatorial Atlantic Oceans are forecast rather better with the GCM than with the statistical model (compare Figures 3(a) and (c)), which includes persistence and ENSO teleconnections. However, over land the skill tends to be lower than over the ocean. In northern South America and along the North American northwest coast one sees well-known ENSO teleconnections. The model Pacific North American (PNA) like teleconnection pattern to North America (Figure 3(b)) is shifted with respect to the observed one (Figure 3(d)), leading to low pointwise correlations away from the coast.

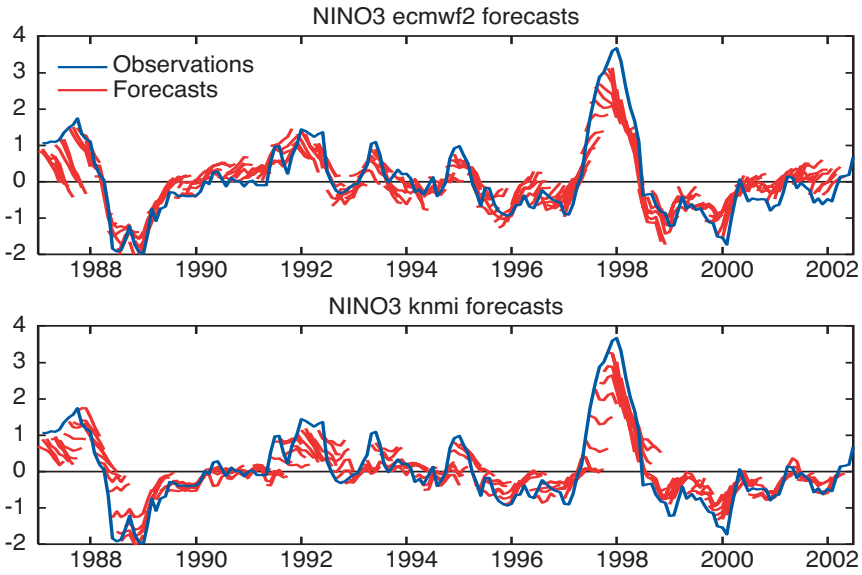

Figure 1 Six-month hindcasts of the Niño3 index of the strength of El Niño (positive) and La Niña (negative) over 1987–2001 of the current ECMWF model (top) and a non-local statistical model (bottom).

The apparent skill over Europe for October starts is replaced by negative skill in the 1 November starts, so could easily be a chance fluctuation.

Precipitation forecasts

Precipitation forecasts are verified against the gridded Global Precipitation Climatology Project (GPCP) merged satellite and rain gauge precipitation analyses. The skill in precipitation forecasts is significantly enhanced by ENSO. This is shown in Figure 4. We computed the skill in three-month averaged precipitation at lead-time +2 months (months 3–5) as a spatial anomaly correlation, and plotted the result against the value of the Niño3 index averaged over the same three months. It is clear that the skill is larger during El Niño or La Niña than during the neutral conditions.

The strongest effects of ENSO on precipitation occur in eastern Indonesia and the western Pacific during the dry season (August–November). The ECMWF model has skill, reaching acc = 0.8 in these areas, see Figure 5. These skills are higher than the model teleconnections and the STAT model skill (where there is enough data), indicating that there is more than Niño3 giving rise to predictability. In Australia one sees reasonable skill along the east coast. However, the model overextends the teleconnection toward the west, leading to forecasts without skill in other parts of Australia.

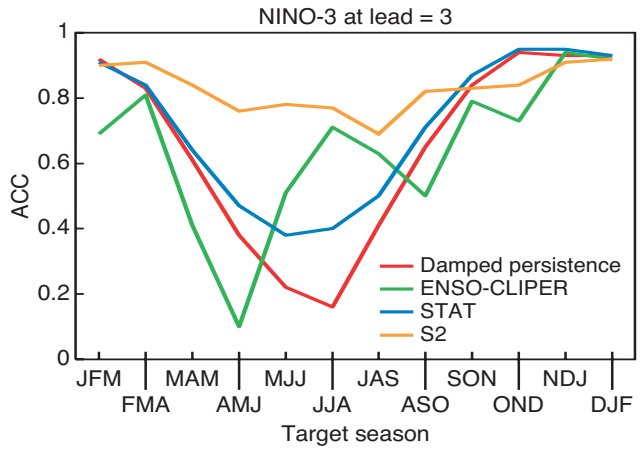

Figure 2 The skill measured by the anomaly correlation coefficient (ACC) at lead-time +3 of the three-month averaged Niño3 index forecast (months 4–6 in ECMWF conventions). The ECMWF forecast (S2) is contrasted with various statistical forecast methods (STAT, ENSO-CLIPER, and damped persistence).

The extratropical teleconnections are strongest in the Americas in December–January. The skill of the 1 October starts is shown in Figure 6(a). The historical teleconnection patterns are reproduced well in Florida, northern South America and southern Brazil (Figure 6(b)). The El Niño related rainfall along the coast of Ecuador and northern Peru was also forecast well by the ECMWF model, whereas the linear statistical model did not see a strong enough historical teleconnection to base forecasts on. On the west coast of the USA the ECMWF model reproduced the long-term historical pattern of no ENSO effects. In contrast, the teleconnections observed over 1987–2002 were quite strong. Possible long-term changes in ENSO teleconnections are a complicating factor, both in making statistical forecasts and in assessing the performance of the ECMWF model. To what extent should we expect the model to reproduce the long-term behaviour, and to what extent should we expect it to mimic the particular behaviour of a recent period?

Overall view

Due to the limited number of years in the verification period, few of the differences between the ECMWF and statistical forecasts noted above are significant. We enhanced the statistical power of the comparison by combining the precipitation forecasts for 40 regions and seasons where we expected skill due to ENSO teleconnections. The results are shown in Figure 7 for a lead-time of two months (other lead times give very similar figures). In 32 out of these 40 cases the ECMWF model performed better than the statistical model. This result is very unlikely to be due to chance, implying that the ECMWF model performs better overall than this statistical model.

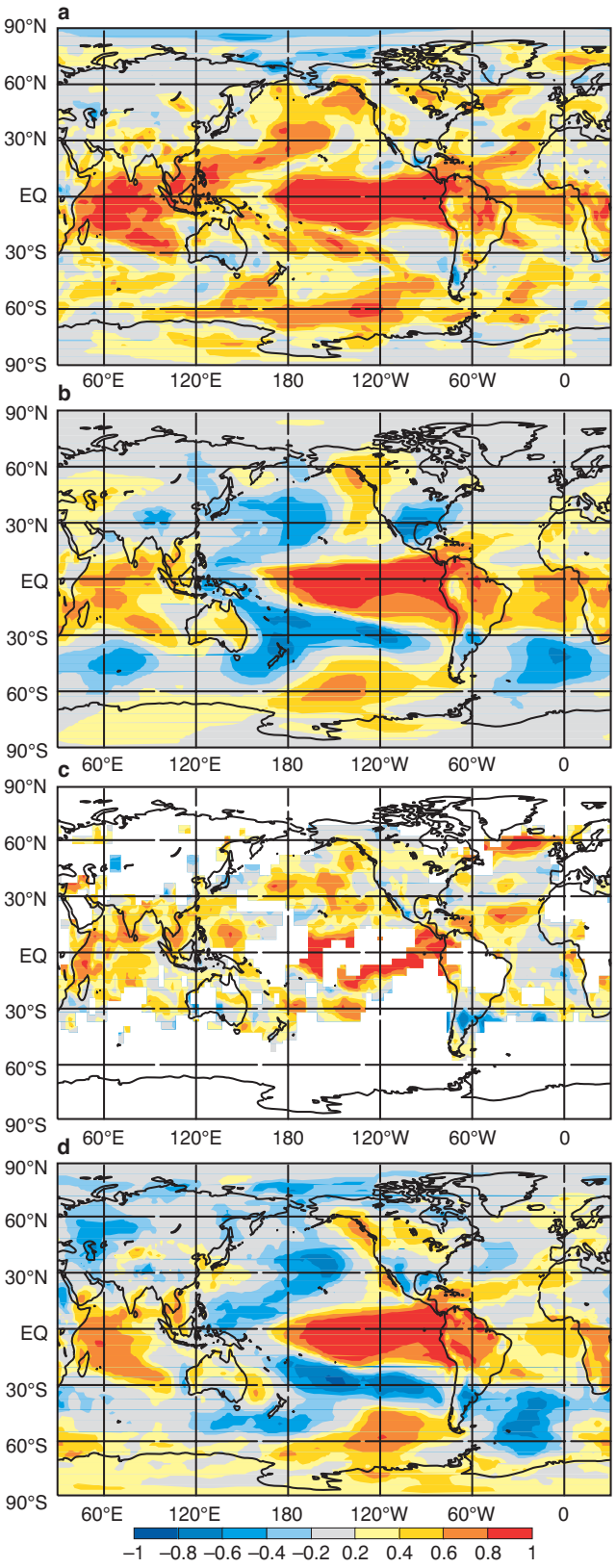

Figure 3 (a) The anomaly correlations of December–February two-metre temperatures from S2 October starts with the NCEP/NCAR reanalysis, (b) the ECMWF S2 teleconnection patterns, (c) the skill of the statistical model (white points did not have enough data or strong enough teleconnections to make a prediction), and (d) the observed teleconnection patterns.

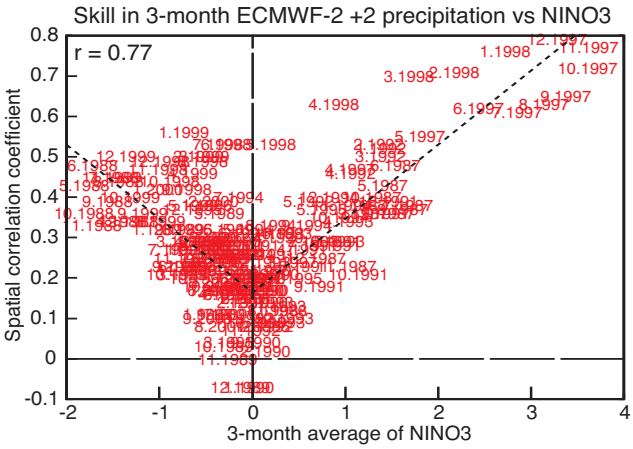

Figure 4 The skill of the precipitation forecasts (spatial correlation of the global ECMWF +2 three-month ensemble mean anomaly with the Global Precipitation Climatology Project observations) as a function of the value of the Niño3 index. The numbers denote the starting month and year of the three-month season.

Conclusions

The performance of the ECMWF seasonal forecasts has been compared with that of a simple, but global, statistical model. The ECMWF forecast model is shown to be better, on average, than this statistical model in

- predicting El Niño through the spring barrier,
- predicting SST in the Indian and Pacific Oceans,
- forecasting rain in areas of known ENSO teleconnections.

Many other aspects of performance have not been investigated here, particularly in mid-latitudes. Nonetheless, our results show that there is already a significant number of seasonal forecast 'targets' where the ECMWF numerical model is outperforming straightforward statistical techniques. More details of this study can be found in the paper by *van Oldenborgh et al.* (2003). All correlation maps have been produced by the KNMI Climate Explorer (http://climexp.knmi.nl). Readers are invited to investigate the skill in other areas and seasons using this public web site.

Further reading

Anderson, **D.L.T.** ***et al.***, 2003: Comparison of the ECMWF seasonal forecast systems 1 and 2, including the relative performance for the 1997/8 El Niño, *ECMWF Technical Memorandum 404*

Landsea, **C.W.**, and **J.A. Knaff**, 2000: How much skill was there in forecasting the very strong 1997-98 El Niño?, *Bulletin American Meteorological Society*, 81, 2107-2119

van Oldenborgh, **G. J.** ***et al.***, 2003: Did the ECMWF seasonal forecast model outperform a statistical model over the last 15 years? *ECMWF Technical Memorandum 418*

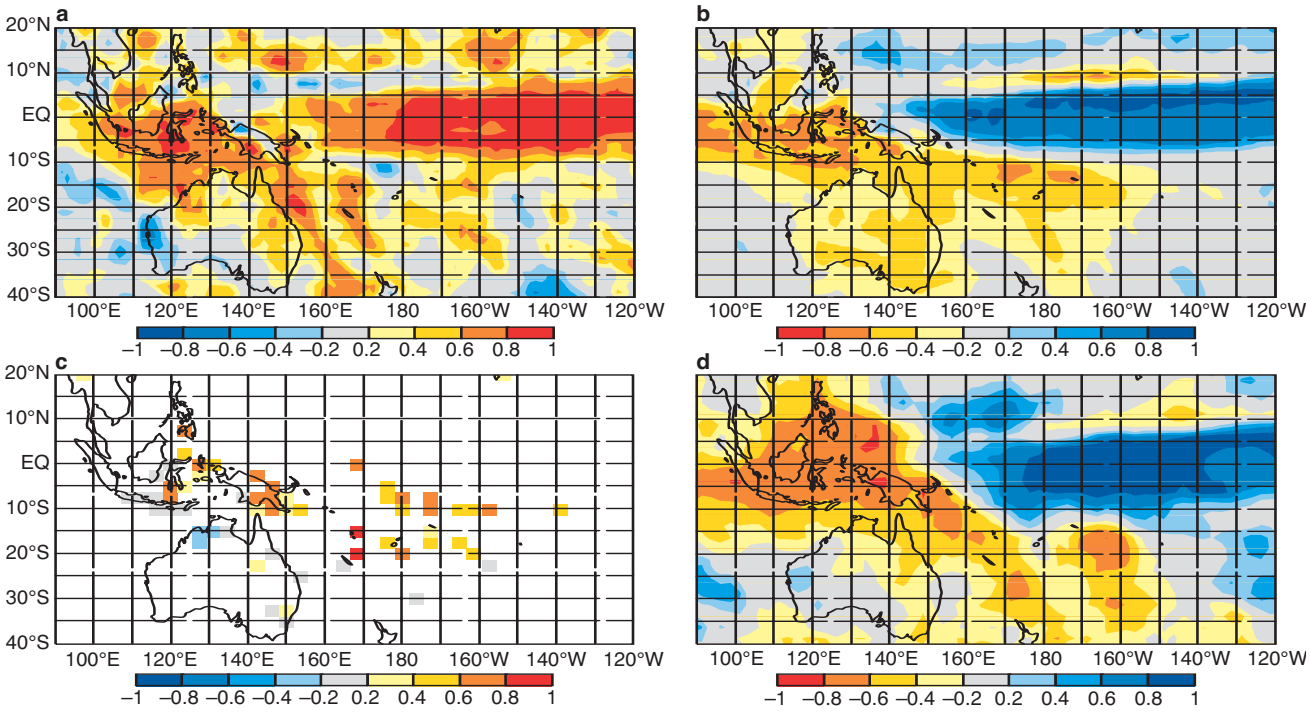

Figure 5 (a) The anomaly correlations of west Pacific dry season (August–November) precipitation from 1 June S2 start with Global Precipitation Climatology Project observations, (b) the S2 teleconnections, (c) the skill of the STAT model and (d) the observed teleconnections.

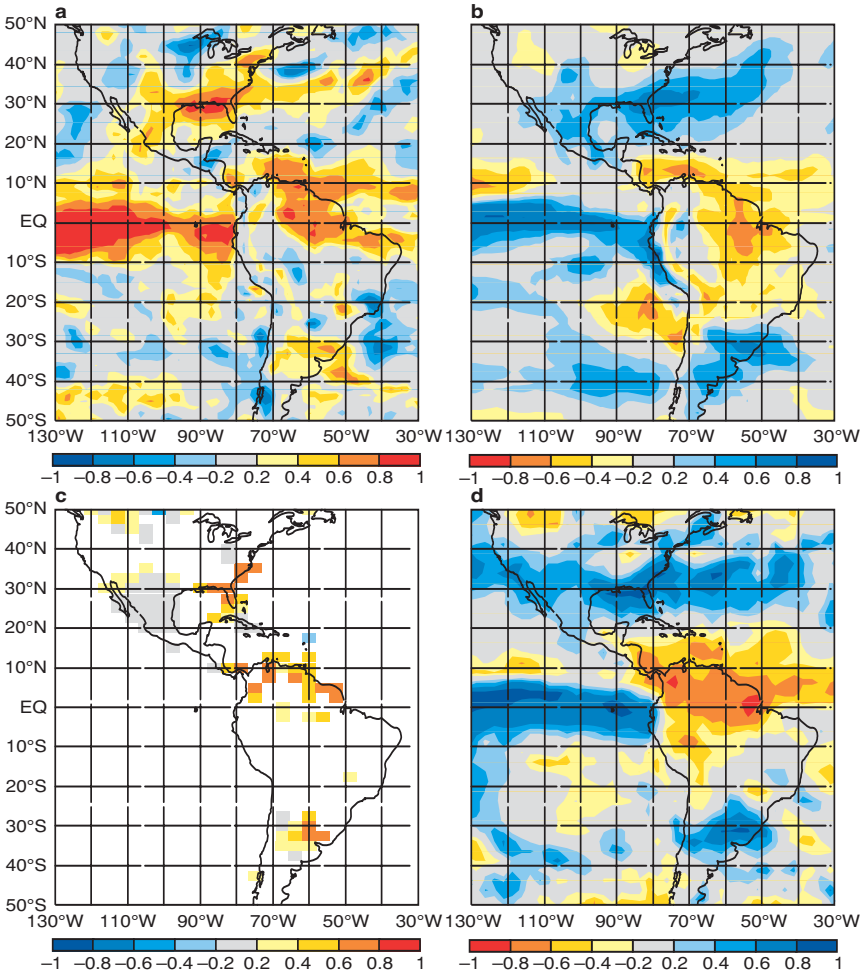

Figure 6 (a) Anomaly correlations of December–February precipitation in the Americas from 1 June S2 starts with Global Precipitation Climatology Project observations, (b) S2 teleconnections, (c) skill of the STAT model, and (d) observed teleconnections.

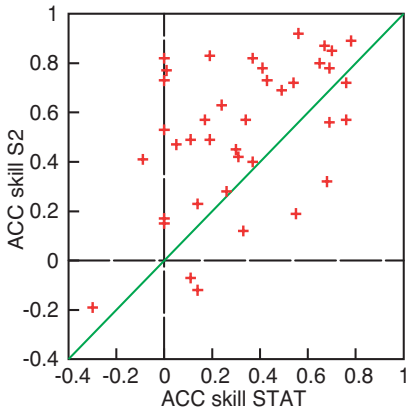

Figure 7 The anomaly correlation coefficient skill score of the +2 month precipitation forecasts of the ECMWF seasonal forecast model (S2) versus that of the statistical model (STAT) for 40 regions and seasons where skill is expected due to ENSO teleconnections.

Geert Jan van Oldenborgh (KNMI), Magdalena Balmaseda, Laura Ferranti, Tim Stockdale & David Anderson (ECMWF)

Record-breaking warm sea surface temperature of the Mediterranean Sea

During the month of May 2003 a warm positive anomaly built up quickly in the sea surface temperature (SST) of central Mediterranean basin. After a short break at the end of May, the anomaly started to grow further and rapidly became very large in the first week of June. Since then the area covered by the anomaly has expanded and at the end of July affected the whole basin (with the exception of the Aegean Sea) leading to sea surface temperatures persistently and uniformly much warmer (order 2–3°C) than climatology. As an example, Figure 1 displays the Mediterranean SST at the end of July and its anomaly with respect to climate (updated daily at http://www.ecmwf.int/products/forecasts/d/charts/analysis).

The unusual persistence and amplitude of such anomalies was noticed as part of the daily monitoring of meteorological fields. The recently completed ERA-40 dataset facilitates the comparison of current conditions with the historical data for the previous 45 years. Figure 2 shows the time series of SST monthly means, averaged over the Mediterranean basin between 0°E and 30°E for March, April and May, as used by ERA-40 (1958–2002). While March and April 2003 were close to the average mean temperature of previous years, May 2003 exceeded the highest value of the previous 45 years. Figure 3 shows the same as Figure 2 but for the summer months June, July and August. Comparison of overlapping years shows that operational SST analyses are in good agreement with ERA-40 SST. Therefore, the departures from climate observed this year couldn't be explained by the usage of different analyses techniques in the two datasets. The monthly value reached in June and July this year is much higher than usual and outside the range of variability exhibited in the previous 45 years; June is almost as high as a normal July and July is as warm as the warmest August in the time series (climatological maximum). At the time of writing, a comparison for August was not yet available.

It is not the purpose of this note to discuss the possible impact of the SST anomalies on the weather affecting the neighbouring regions. Nevertheless, the ERA-40 dataset suggest a persistence of summer SST anomalies into the autumn. A warmer Mediterranean can lead to heavier rain events and increased intensity of Mediterranean cyclogenesis, as suggested by previous works (see articles cited below).

Finally, it is worth mentioning that the SST anomaly is not restricted only to Mediterranean waters but also affects northern Europe where sea basins and lakes are experiencing very warm conditions. The Baltic and the North Sea are much warmer than usual and the temperature of the major lakes in Finland is between 4°C and 6°C warmer than its climatological mean. (http://www.ymparisto.fi/eng/environ/monitor/hydro/temperat.htm).

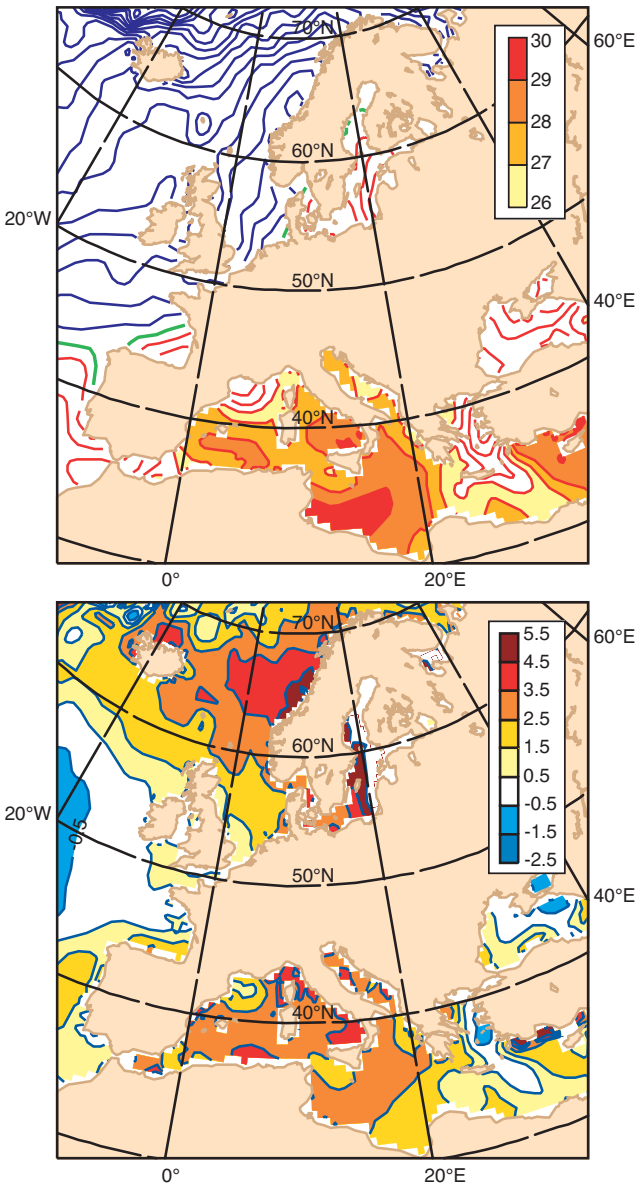

Figure 1 (a) The operational analysis of sea surface temperature for 31 July 2003. The contours are every 1°C, the green line is the 20°C isoline while sea surface temperature above 26°C is shaded. (b) The anomaly with reference to a subset of ERA-40 dataset on the same day. The anomalies are shaded at 1°C intervals starting from 0.5°C (positive) and –0.5°C (negative).

Articles about the meteorological impact of warm Mediterranean sea-surface temperatures

Trigo, I.F., G.R. Bigg & **T.D. Davies**, 2002: Climatology of cyclogenesis mechanisms in the Mediterranean. *Monthly Weather Review*, **130**, 549–569.

Pastor, F., M.J. Estrela, D. Peñarrocha & **M.M. Millán**, 2001: Torrential rains on the Spanish Mediterranean coast: modelling the effects of the sea surface temperature. *Journal Applied Meteorology*, **40**, 1180–1195

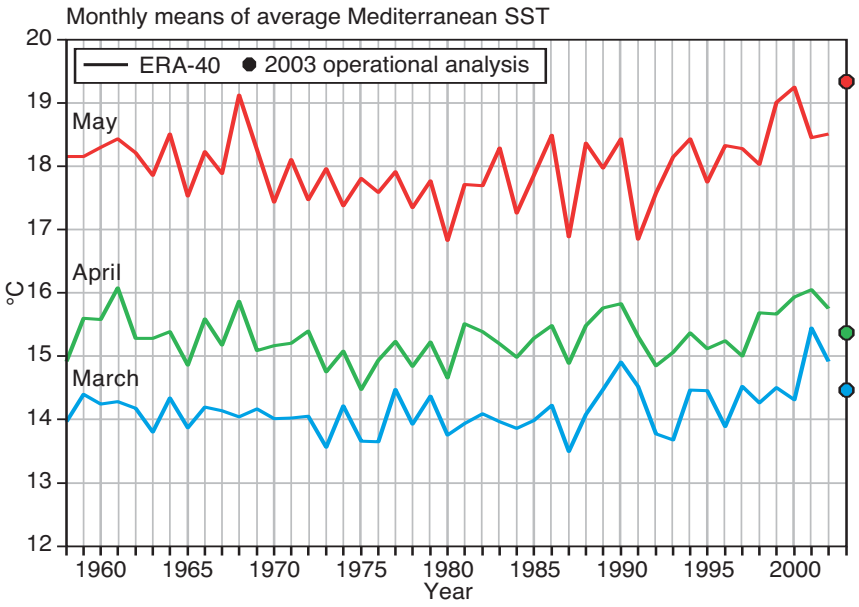

Figure 2 The time series of monthly-mean sea surface temperature, averaged over the Mediterranean basin between 0°E and 30°E, for March (cyan line), April (green line) and May (red line) from ERA-40 (1958-2002). The dots represent this year's monthly mean computed from the operational analyses.

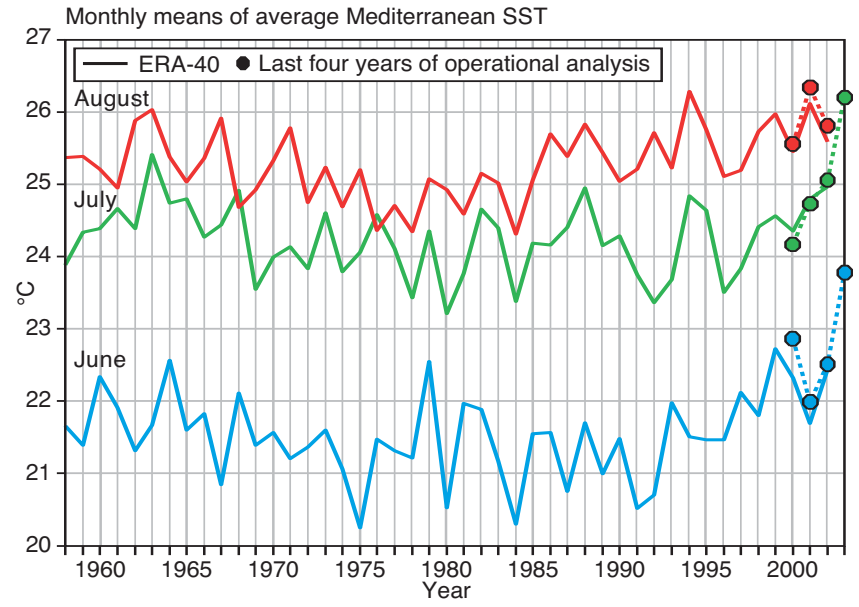

Figure 3 As Figure 2, but for the summer months June (cyan line), July (green line), August (red line). The dots represent the monthly means computed from recent operational analyses.

Federico Grazzini & Pedro Viterbo

New ECaccess features

The ECaccess portal has been enhanced to provide access to the Centre's computing and archiving facilities via the RMDCN network. A second ECaccess server has been installed. Member States' and Co-operating States' ECaccess Gateways can use either the Internet or the RMDCN server. The new portal is available at msaccess.ecmwf.int

The following additions have been made recently to the ECaccess services. All these functions are available through the ECaccess Gateway version 2.0.3.

Virtual Network Computing – VNC

Support for Virtual Network Computing has been added. VNC allows X11 applications to be started on a Windows workstation. It is an easy-to-install thin client application, is faster than a normal X11 emulator and is available free of charge. The X11 session can be started through the VNC viewer, using the 'ecxterm-vnc' command.

Secure SHell – SSH

SSH provides users with a secure login to remote systems. It also allows secure X11 and VNC connections to be opened. An SSH plug-in has been developed and ECaccess now offers this service through the ECMWF Internet gateway, ecaccess.ecmwf.int. Files transfer will be offered in a next release.

ECtrans enhancements

ECtrans allowed secure file transfers from ECMWF to remote servers. It is now possible to use the 'ectrans' command

also in the opposite direction to transfer files from remote servers to ECMWF. SFTP has been added to the list of protocols supported by ECtrans to transfer files through the ECaccess Internet server. It is now possible to use the 'ectrans' command to transfer files with SSH servers. The option to perform synchronous transfers, bypassing the ECtrans spool, has also been added.

Management module

Additional functions have been added to the administration module, allowing users to manage easily their ECtrans configuration and destination. These functions are available through the ECtrans set-up menu of the ECaccess web interface.

MARS Access

The MARS archive is now accessible through the ECaccess portal. Modified versions of the stand-alone MARS client, which interfaces with ECaccess, can be downloaded from www.ecmwf.int/services/archive/download.html. MARS requests can also be managed interactively via the ECaccess FTP server. For users accessing MARS remotely via Metview, the MARS remote module for Metview is also available. This module can be downloaded from www.ecmwf.int/services/archive/download.html

For a full description of ECaccess, please refer to the ECMWF Newsletter 96 – Winter 2002/03, available at www.ecmwf.int/publications/newsletters/pdf/96.pdf.

For more information on the ECaccess portal, please contact your usual User Support Contact Point.

Matteo Dell'Acqua & Laurent Gougeon

ECMWF publications

A full list of ECMWF publications is available at
http://www.ecmwf.int/publications/library/ecpublications/
and recently published Technical Memoranda can be downloaded in pdf format from
http://www.ecmwf.int/publications/library/ecpublications/techmemos/tm00.html

Technical Memoranda

398 **M.M. Coutinho, B.J. Hoskins & R. Buizza**: The influence of physical processes on extratropical singular vectors. *April 2003*

401 **C. Keil & C. Cardinali**: The ECMWF Re-Analysis of the Mesoscale Alpine Programme Special Observing Period. *March 2003*

404 **D. Anderson, T. Stockdale, M. Balmaseda, L. Ferranti, F. Vitart, P. Doblas-Reyes, R. Hagedorn, T. Jung, A. Vidard, A. Troccoli & T. Palmer**: Comparison of the ECMWF seasonal forecast Systems 1 and 2, including the relative performance for the 1997/8 El Niño. SAC Report *September 2002/April 2003*

405 **N. Wedi & P. Smolarkiewicz**: Extending Gal-Chen and Somerville terrain-following coordinate transformation on time-dependent curvilinear boundaries. *April 2003*

406 **S. Abdalla & H. Hersbach**: Interim report on the technical support for global validation of ERS wind and wave products at ECMWF. *April 2003*

407 **L. Isaksen & P.A.E.M. Janssen**: Impact of ERS scatterometer winds in ECMWF's assimilation system. *May 2003*

408 **L. Cavaleri & L. Bertotti**: The improvement of modelled wind and wave fields with increasing resolution. *June 2003*

409 **L. Cavaleri & L. Bertotti**: The accuracy of modelled wind and waves fields in enclosed seas. *June 2003*

412 **E. Moreau, P. Lopez, P. Bauer, A. Tompkins, M. Janisková & F. Chevallier**: Variational retrieval of temperature and humidity profiles using rain rates versus microwave brightness temperatures. *July 2003*

NWP Satellite Application Facility Technical Report

№ 8 **F. Chevallier, P. Lopez, A.M. Tompkins, M. Janisková & E. Moreau**: The capability of 4D-Var systems to assimilate cloud-affected satellite infrared radiances. *July 2003*

ERA-40 Project Report Series

№ 6 **A.K. Betts, J.H. Ball & P. Viterbo**: Evaluation of the ERA-40 surface water budget and surface temperature for the Mackenzie River basin. *April 2003*

№ 7 **A.K. Betts, J.H. Ball, M. Bosilovich, P. Viterbo, Y. Zhang & W.B. Rossow**: Intercomparison of water and energy budgets for five Mississippi sub-basins between ECMWF Reanalysis (ERA-40) and NASA-DAO fvGCM for 1990-1999. *June 2003*

EUMETSAT/ECMWF Fellowship Programme Research Report

№ 13 **N. Bormann & J-N. Thépaut**: Impact of MODIS polar winds in ECMWF's 4D-Var data assimilation system. *May 2003*

Workshop proceedings

ECMWF/GEWEX workshop on humidity analysis, *8-11 July 2002*

ECMWF calendar 2003

Sep 8–12	**Seminar** – *Recent developments in data assimilation for atmosphere and ocean*	
Oct 2	**Advisory Committee of Co-op States**	*10th*
Oct 6–8	**Scientific Advisory Committee**	*32nd*
Oct 8–10	**Technical Advisory Committee**	*33rd*
Oct 13–14	**Finance Committee**	*71st*

Meteorological Training Course for WMO members

Oct 13–17	**Use & interpretation of ECMWF products**	
Oct 15	**Advisory Committee on Data Policy**	*4th*
Oct 21–22	**Policy Advisory Committee**	*19th*
Nov 3–6	**Workshop** – *Simulation and prediction of intra-seasonal variability*	
Nov 10–14	**Workshop** – *Meteorological operational systems*	*9th*
Dec 2–3	**COUNCIL**	*59th*

Index of past newsletter articles

This is a list of recent articles published in the ECMWF Newsletter series. Articles are arranged in date order within each subject category. Articles in red can be accessed on the ECMWF public web site http://www.ecmwf.int/pressroom/newsletter/index.html

New products on the ECMWF web site

Research Data Server

Two new datasets have been added to the ECMWF Data Server: 450 Gb of data from the 40-year ECMWF Re-analysis (ERA-40) project and data from the ENhAnced ocean data assimilation and ClimaTe prediction (ENACT) project. The ECMWF Data Server provides free access for research use to publicly released datasets.

http://data.ecmwf.int/data/

Data Services on-line ordering

A new version of the Data Services On-line system has been made available with improvements in the facilities for finding data (DataFinder). The handling charges of the archived data are now based on a new costing algorithm that reduces the costs of the archived-data orders. Also, the 40-year ECMWF Re-analysis (ERA-40) data sets have been added to the on-line catalogue.

http://www.ecmwf.int/products/data/ds/

GRIB data

GRIB decoding software version 220 was released on 28 May 2003, which includes modifications to enable compilation using the g77 Fortran compiler under Linux.

http://www.ecmwf.int/products/data/software/

Observational data monitoring

The ECMWF Global Monthly Monitoring Report on observations is now published and updated in html and pdf formats.

http://www.ecmwf.int/products/forecasts/monitoring/mmr/

Forecast Users Meeting

Presentations and summaries from the medium-range forecast and seasonal forecast users meetings (16-17 and 18-19 June 2003) have been posted in html and pdf format.

http://www.ecmwf.int/publications/member_states_meetings/

ECMWF Library

The ECMWF Library web pages have been updated. The pages containing reference lists are now produced dynamically. This means that the information is drawn from the Library database of bibliographic entries in real-time.

http://www.ecmwf.int/publications/library/

Annual Seminar 2003

The 2003 ECMWF Annual Seminar is titled 'Recent developments in data assimilation for atmosphere and ocean' and runs from 8-12- September at ECMWF.

http://www.ecmwf.int/newsevents/meetings/annual_seminar/

Workshops

The following workshops have been held recently or are scheduled:

- 9th Workshop on meteorological operational systems;
- Workshop on simulation and prediction of intra-seasonal variability;
- Workshop on modelling and assimilation for the stratosphere and tropopause.

http://www.ecmwf.int/newsevents/meetings/workshops/

Andy Brady

Useful names and telephone numbers within ECMWF

Telephone number of an individual at the Centre is:

International: +44 118 949 9 + three digit extension
UK: (0118) 949 9 + three digit extension
Internal: 2 + three digit extension

e.g. the Director's number is:
+44 118 949 9001 (international),
(0118) 949 9001 (UK) and 2001 (internal).

E-mail

The e-mail address of an individual at the Centre is:
firstinitial.lastname@ecmwf.int

e.g. the Director's address is: D.Burridge@ecmwf.int

Internet web site

ECMWF's public web site is: http://www.ecmwf.int

	Ext
Director	
David Burridge	001
Deputy Director and Head of Operations Department	
Dominique Marbouty	003
Head of Administration Department	
Gerd Schultes	007
Head of Research Department	
Philippe Bougeault	005
ECMWF switchboard	000
Advisory	
Internet mail addressed to Advisory@ecmwf.int	
Telefax (+44 118 986 9450, marked User Support)	
Computer Division	
Division Head	
Walter Zwieflhofer	050
Computer Operations Section Head	
Sylvia Baylis	301
Networking and Computer Security Section Head	
Matteo Dell'Acqua	356
Servers and Desktops Section Head	
Richard Fisker	355
Systems Software Section Head	
Neil Storer	353
User Support Section Head	
Umberto Modigliani	382
User Support Staff	
John Greenaway	385
Norbert Kreitz	381
Dominique Lucas	386
Carsten Maaß	389
Pam Prior	384
Computer Operations	
Call Desk	303
Call Desk email: cdk@ecmwf.int	
Console - Shift Leaders	803
Console fax number +44 118 949 9840	
Console email: newops@ecmwf.int	
Fault reporting - Call Desk	303
Registration - Call Desk	303
Service queries - Call Desk	303
Tape Requests - Tape Librarian	315
Software libraries (eclib, nag, etc.)	
John Greenaway	385

	Ext
ECMWF library & documentation distribution	
Els Kooij-Connally	751
Meteorological Division	
Division Head	
Horst Böttger	060
Applications Section Head	
Alfred Hofstadler	451
Data and Services Head	
Baudouin Raoult	404
Graphics Section Head	
Jens Daabeck	375
Operations Section Head	
François Lalaurette	420
Meteorological Analysts	
Antonio Garcia Mendez	424
Federico Grazzini	421
Anna Ghelli	425
Meteorological Operations Room	426
Data Division	
Division Head	
Adrian Simmons	700
Data Assimilation Section Head	
Erik Anderson	627
Satellite Section Head	
Jean-Nöel Thépaut	621
Reanalysis Project (ERA)	
Saki Uppala	366
Probability Forecasting & Diagnostics Division	
Division Head	
Tim Palmer	600
Seasonal Forecasting Head	
David Anderson	706
Model Division	
Division Head	
Martin Miller	070
Numerical Aspects Section Head	
Mariano Hortal	147
Physical Aspects Section Head	
Anton Beljaars	035
Ocean Waves Section Head	
Peter Janssen	116
Education & Training	
Renate Hagedorn	257
GMES Coordinator	
Anthony Hollingsworth	824